A Study of Axisymmetric Submerged Semi-Turbulent Jets

El Sayed Aly, Mohamed Nezam

A Dissertation

IN THE

FACULTY OF ENGINEERING

Presented in Partial Fulfillment of the Requirements for the Degree of MASTER OF ENGINEERING

at

CONCORDIA UNIVERSITY

Montreal, Quebec

MARCH 1977

ABSTRACT

EL SAYED ALY, MOHAMED NEZAM

A STUDY OF AXISYMMETRIC SUBMERGED SEMI-TURBULENT JETS

The region near the nozzle exit of free jets is of interest to designers of fluid control and free jet sensing devices.

An experimental investigation of an axially symmetric semi-turbulent jet has been carried out in the region close to the nozzle for jet Reynolds numbers of 2937 and 1072. The experimental results are compared with solutions based on Schlichting's classical method {1} Abramovich's method {2} and with the solution reported by Hinze {15}.

It is shown that Schlichting's solution does not give accurate predictions within 1 to 21 diameters from the nozzle even after the expression for the virtual origin has been adjusted to correspond more closely to measurements in the far region of the jet. Abramovich's solution also does not represent the predictions of the velocities within 1 to 18 diameters from the nozzle. Better agreement is obtained with Hinze's solution when the virtual origin and the kinematic viscosity are adjusted to intermediate values between laminar and turbulent flows.

/. . .

ACKNOWLEDGMENT

The author wishes to express his gratitude to his supervisor, Dr. M.P. duPlessis, for his support and guidance throughout this study.

TABLE OF CONTENTS

LIST OF FIGURES

NOMENCLATURE

A	coefficient used in an empirical equation for determining the anemometer output voltage
a	overheat ratio
B	coefficient used in an empirical equation for determining the anemometer output voltage
b	film width
$b_{0.5}$	half-velocity width
c	velocity coefficient
c	constant
d	diameter of the nozzle exit, in.
E	anemometer output voltage, volt
F	constant
g	gravity, ft./sec.^{2}
h	constant head, in.
	momentum of the jet flow in x direction, lb.
Kg	heat conductivity of glass support
k	jet momentum/density of fluid
K	heat conductivity of fluid
n	constant
R	radius of the nozzle exit, in.
R'	mamometer reading, in.
r	radial coordinate, in.
Δr	positioning error
S_o	specific gravity of mercury
S	specific gravity of the oil
t	time in seconds, sec.
T	temperature ^oF

u	axial velocity component, ft./sec.
U_o	initial center-line velocity. ft./sec.
U_m	mean velocity of the jet at the nozzle exit, ft./sec.
U_{max}	center-line velocity of the jet, ft./sec.
$\Delta U_{1,2,3}$	velocity errors, ft./sec.
x	axial coordinate, in.
x_o	virtual origin distance, in.
x	axial coordinate referred to the virtual origin, in.
xo_h	distance from nozzle tip to intersection of boundary layer edges, in.
x_n	distance between the nozzle exit and the beginning of the main region, in.
x_h	the length of the initial region from the nozzle exit, in.
Y_1	the location of the edge of the constant velocity core from the nozzle surface, in.
Y_2	the location of the edge of the jet boundary layer to the nozzle surface, in.
Z	function of the velocity parameter
Z'	First derivative of Z w.r.t. ϕ
ρ	density of the fluid, lb.sec.^{2}/ft.^{4}
μ	absolute viscosity of the fluid
ε_o	virtual kinematic viscosity for turbulent flow, ft.^{2}/sec.
ν	kinematic viscosity of the fluid, ft.^{2}/sec.
Re	Reynolds number
Cp	specific heat at constant pressure
α	constant
β	momentum flux coefficient

γ film temperature coefficient $(^{o}C)^{-1}$

η similarity parameter

ψ dimensionless velocity u/U_{max}

ϕ velocity parameter

INTRODUCTION

The region near the nozzle exit of free jets is of interest to designers of fluid control and free jet sensing elements.

Previous studies have dealt mainly with laminar and turbulent jets. To date little work has been carried out with semi-turbulent jets with Reynolds numbers between 1000 and 3000.

The present work is an experimental investigation of an axisymmetric semi-turbulent oil-to-oil jet issuing from a long tube in which the flow is fully developed.

The objective of the study is to establish to what extent existing solutions with the virtual origin expression can be used to predict the semi-turbulent jet characteristics.

CHAPTER 1

A REVIEW OF PREVIOUS WORK ON SUBMERGED FREE JETS

1.1 Jet types

The flow characteristics of a jet depends upon the exit Reynolds number and on the velocity profile at the nozzle exit.

Reynolds [9] observed that "for fully developed pipe flow in the nozzle, progressively longer laminar jets can be maintained as Reynolds number increases towards 150. For higher Reynolds numbers still longer simple jets can exist, but a complex breakdown can also occur with a reduction in length of the simple jet as Reynolds number increases towards 300".

McNaughton and Sinclair [11] studied the problem extended to higher Reynolds numbers and they identified four main types of jets:

a - dissipated laminar jet (Re < 300 approx.)

b - fully laminar jet (300 < Re < 1000)

c - semi-turbulent jet (1000 < Re < 3000)

d - fully turbulent jet (Re > 3000)

They noted that the distance between the nozzle exit and the location where the jet breaks up into turbulence decreases as Re increases from 300.

The Reynolds number range defining the different types of jets is affected by the external conditions such as vibrations and acoustic interference.

1.2 Laminar jet break-down phenomenon [10]

The origin of the disturbances is the free shear layer which causes the laminar jet break-down phenomenon.

The shear layer is unstable to infinitesimal disturbances at almost any Reynolds number greater than a critical value as soon as a point of inflexion appears in the velocity profile. The critical Reynolds number is obtained from hydrodynamic stability analysis of the laminar jet.

The point of inflexion exists in the flow immediately after the jet leaves the nozzle, the frequency of the primary disturbance depends on the velocity gradient of the boundary layer at the nozzle wall.

As the primary wave propagates down-stream, it gains energy from the main flow and eventually forces the jet to follow a sinuous undulation a few diameters' distance from the exit.

When the undulating fluid at the jet edge cannot sustain the oscillation, the sinuous wave gradually transforms itself into a disturbance of a vortex ring form around the jet. The mean velocity of the region increased towards a critical vortex strength above which the vortices decay irregularly. The vortices finally break up to small disturbances further down-stream and transform the jet into a turbulent one.

The jet will break up earlier at higher Reynolds numbers. McNaughton and Sinclair [11] found that the transition occurs at Reynolds number equal to 1000.

CHAPTER 2

EXPERIMENTAL WORK

2.1 Axisymmetric turbulent jet flow system

A schematic diagram of the oil flow system used in the experiment is shown in Fig. (1). The flow supply is derived from a pump. Outflow from the pump is manually regulated by two needle valves, main and bypass. Any irregular flow pattern caused by the valves is smoothed out by an aluminum settling chamber (8 in. dia. X 3 ft. long) positioned immediately downstream of the main valve.

The nozzle at the outlet of the setting chamber consists of a convergent section and a circular aluminum tube (0.824 inch I.D. X 3 ft. long). The tube length satisfies the condition $\frac{L}{d} = 0.03$ Re up to Re = 1600 for fully developed laminar flow reported by Schlichting [1] and $\frac{L}{d} = 25 - 40$ for fully developed turbulent flow through pipes reported by J. Nikuradse [14].

Efflux from the nozzle emerges into an oil-filled, open steel tank to form an axisymmetric submerged jet.

The tank is 4 ft. wide X 4 ft. high X 5.5 ft. long and has the capacity to contain 665 gallons of oil.

A screen made of pressed animal hair (commonly used for packaging) sandwiched between perforated aluminum plates, is located in front of the overflow weer to distribute the flow evenly over the tank cross-section.

2.2 Velocity measurement apparatus

A three-directional traversing mechanism for velocity measurements is mounted above the tank on machined tracks fixed to the side plates of the tank. A transit and cathetometer were used to align the traversing mechanism with the axis of the circular tube and to ensure that the three traversing directions are mutually perpendicular.

The traversing mechanism is equipped with a probe holder having a 3/4-in. dia. X 4-ft.-long aluminum tube extension to protect the electrical cable connected to the hot-film probe from the oil. Measurements of the velocities parallel to the axis direction are taken with a hot-film probe (DISA type 55 R 36) which is clamped in the traversing mechanism and which can be located at any point in the jet flow field with a maximum position error of ±0.06 in.

The probe is used with a DISA type 55 D 01 constant temperature anemometer and readings are taken directly from a d-c voltmeter which has an accuracy of 1.0 percent full scale in the range of zero to 20 volts.

The range of probe measurements is:

Minimum velocity	0.033	ft./sec.
Maximum velocity	82.5	ft./sec.

In order to ensure steady state operation, readings are taken after 10 minutes of system running for each experiment.

The probe is located at 0.1875 in. from the nozzle exit, the manual valves are controlled to get the anemometer output to correspond to a particular value of Reynolds number close to the upper limit (3000) for semi-turbulent jets.

The output of the anemometer is observed for 2 minutes, the valves are adjusted whenever necessary to maintain the required value of Reynolds number. The probe is then located at one nozzle diameter from the nozzle exit along its center-line and the first reading is taken at the jet center-line.

The probe is relocated in the radial direction at 1.75 in. above the center-line of the jet and a total of 15 readings are taken at intervals of 0.125 in. moving from the outer region towards the jet center-line. Readings are also taken in sequence at 15 locations below the jet center-line to obtain the full jet profile in a vertical plane.

The probe is then relocated at each of the stations along the center-line of the jet and the previous procedure is repeated at each of the stations up to the station $x = 24d$ from the nozzle exit to complete one set of readings at the specified Reynolds number.

The probe then is located again at 0.1875 in. from the nozzle exit, the manual valves are adjusted to get a second value of Reynolds number close to the lower Reynolds number of

1000. The procedure is repeated to get the first set of readings at the second value of Reynolds number.

Thus, readings are taken from one experiment for the two values of the specified Reynolds numbers.

The previous experimental procedure is repeated twice again to get 3 sets of readings for each of the Reynolds numbers (2937 and 1072).

2.3 Hot-film probe calibration

The hot-film probe is calibrated by inserting the probe in an oil jet issuing from a 0.5 in. dia. sharp-edged orifice in a constant pressure tank (4 in. dia. X 3 ft. long)

Oil is delivered to the constant pressure tank by a gear pump driven by a variable speed motor and the pressure in the tank can be maintained at different levels by adjusting the circulation rate.

The system provides constant jet velocities from 5 to 40 ft./sec. The velocity of the flow is verified by means of the pitot tube equation.

$$U = C \left(2 g R' \left(\frac{S_o}{S} - 1 \right) \right)^{0.5} \qquad (2.3.1)$$

The velocity coefficient C is taken as unity

The jet becomes unsteady at low flows and reliable velocity calibrations could not be obtained in this system at velocities less than 5 ft./sec.

Calibration of the probe at velocities from 1 ft./sec. to a 5 ft./sec. is carried out in a jet issuing from a 3/4 in. dia. sharp-edged orifice in a constant head tank.

The jet velocity is calculated from:

$$u = C\ (2\ gh)^{0.5} \qquad (2.3.2)$$

The velocity coefficient is 0.98 for an orifice of the type used.

The heat transfer from a quartz-coated film probe in a flow field is governed by laws of natural convection, forced convection and heat conduction to the film support. The anemometer output voltage E is related to the flow velocity U by the following equations:

$$E^2\ S_1 = S_2 + S_3\ U^{0.5} \qquad (2.3.3)$$

where

$$S_1 = S_1\ (a) \qquad (2.3.4)$$

$$S_2 = S_2\ (Kg,\ Cp,\ \mu,\ K) \qquad (2.3.5)$$

$$S_3 = S_3\ (Kg,\ Cp,\ \mu,\ K,\ \rho,\ b) \qquad (2.3.6)$$

Each symbol is defined in the Nomenclature

For the hot-film probe used in the study with constant temperature, the previous equation can be simplified to:

$$E^2 = A + BU^{0.5} \qquad (2.3.7)$$

The coefficients A and B depend only upon the operating overheat ratio of the film. From the present test at an oil temperature of 70°F the values of A and B are evaluated (by the least square fit method) to be 44.16 and 67.55 respectively for an overheat ratio of 0.6.

The probe is not calibrated at low velocities less than 1 ft./sec. and it is assumed here that the equation holds in the low velocity region.

Fig. {2} shows the velocity profile at the orifice and Fig. {3} shows the calibration curve for the hot-film probe used.

2.4 Oil viscosity measurements

The oil used in the experiment is FAXAM-40, an industrial lubricant oil processed by Esso Imperial Oil Ltd., its kinematic viscosity is 0.0005 ft^2/sec. at 70°F and its specific gravity is 0.872 as supplied by the company.

The viscosity is measured by means of the saybolt viscometer in accordance with the method approved as ASTM standard D88-53. The saybolt viscometer is of the efflux type where a fixed volume of fluid is discharged through a short tube during a measured time interval. The resulting time t for 60 cc of fluid to pass through at a given temperature is called the Saybolt Universal Viscosity (SUV) in seconds. Kinematic viscosity conversion from saybolt universal second (SUS) to a unit in the British system is obtained from

$$\nu \ (\text{ft.}^2/\text{sec.}) = (2.37 \times 10^{-6}) \ t - \frac{1.94 \times 10^{-3}}{t} \qquad (2.4.1)$$

An expression deduced from ASTM standard ASTM D445-53T and ASTM D446-53.

The kinematic viscosity of the oil in SUS determined experimentally is shown in Fig. (4) as a function of the temperature.

The measured value at room temperature is less than the value given by the supplier. For example, an oil temperature of 70°F, the kinematic viscosity determined experimentally, is 0.000444 ft.^{2}/sec. as compared to 0.0005 ft.^{2}/sec. which is about 11.2% less. The experimental value was used in the theoretical prediction of velocity distributions of the axisymmetric oil jet flow.

The measured value of the oil specific gravity at room temperature is 0.8625.

2.5 Accuracy and reliability of velocity readings

The accuracy of velocity measurements depends on two factors, one factor is the accuracy with which the probe location can be determined and the other factor is the accuracy with the probe measures the velocity

The positioning error causes the maximum velocity error where the velocity gradient is greatest i.e. at the nozzle exit. The error is of the type arising from the probe width

(0.0397 in.), which gives an average value of the velocity in the field instead of a point measurement, and the probe location error ($\pm$ 0.06 in.).

Considering the value of the film width, it can easily be shown (4) that the error is given by

$$\frac{\Delta U_1}{U_o} = -\frac{4}{3}\left(\frac{b}{2d}\right)^2 \qquad (2.5.1)$$

Substituting the known values of b = 0.0397 in . and d = 0.824 in., the error is found to have a magnitude of

$$\frac{\Delta U_1}{U_o} = -0.076 ,$$

an order which is negligibly small. The velocity readings can therefore be considered as point measurements.

The positioning error is a more predominant factor in the experimental work. Misplacement of the probe by a few thousandths of an inch, in a region where the velocity gradient is high, can result in fairly large discrepancies between measured and predicted velocity profiles. The magnitude of this error (4) is given by

$$\frac{\Delta U_2}{U_o} = -8\,\Delta r\,\left(\frac{r}{d^2}\right) \qquad (2.5.2)$$

The steel rule on the vertical traverse has an accuracy of $\pm$ 0.06 in. Substituting this value for the positioning error r and putting r= d/2 in., the error is found to have a maximum value of

$$\frac{\Delta U_2}{U_o} = \pm 0.29$$

which is high in view of the actual velocity magnitude near the nozzle wall. Therefore, extreme care was taken during the experiment in positioning the probe.

During each experiment the oil temperature was found to vary not more than $\pm 3^{0}F$. The operating overheat ratio, a, of the probe had an error given by

$$\Delta a = \pm \gamma \Delta T \qquad (2.5.3)$$

For the DISA 55R36 film probe, the film has a temperature coefficient, $\gamma = 0.003 \ (^{o}c)^{-1}$. The error $\Delta a = 0.005$ is small compared to the value of $a = 0.60$. Hence the coefficients A and B in Equation (2.3.7) should remain practically constant for each test. However, the numerical value of B could have an error, arising from a misinterpretation of the slope from the calibration curve.

The magnitude of the accuracy of the velocity readings can be deduced from the following equation:

$$\Delta U_3 = \frac{4E\ (E^2 - A)}{B^2}\ \Delta E - \frac{2\ (E^2 - A)}{B^3}\ \Delta B \qquad (2.5.4)$$

which was obtained by differentiating Equation (2.3.7).

It is estimated that $\Delta B = \pm 0.2$ with the accuracy of the digital voltmeter $\Delta E = \pm 0.01$ volt, Equation (2.5.4) becomes

$$\Delta U_3 = \pm 8.766\ (10^{-6})\ E(E^2 - 44.16) \pm 1.2977(10^{-6})\ X\ (E^2 - 44.16) \qquad (2.5.5)$$

Equation (2.5.5) shows that the accuracy of U is dependent on the value of E.

For the velocity range under investigation, the maximum value of E did not exceed 18.40 volts. Therefore, ΔU_3 has a maximum value of 0.048 f.p.s. and the accuracy improves as E decreases.

From the tabulated readings (Appendix 1). We can see that the center-line velocity at the nozzle exit is the same in the three different experiments for each value of Reynolds numbers of 1072 and 2937.

The velocity readings are slightly different at the same point for each experiment in the down-stream direction.

Appendix 2 gives the average velocities and the maximum percentage deviation from the average at each point.

For example; for Re = 2937 at the nozzle exit, at the station x/d = 1, the maximum percentage deviation at the point r/d = 0.0 is 0.0%, while the maximum percentage deviation at the point r/d = 1.25 is 7.2%.

At the station x/d = 12, the maximum percentage deviation of the point r/d = 0.0 is 2.9%, while the maximum percentage deviation at the point r/d = 1.25 is 3.9%.

At the station x/d = 24, the maximum percentage deviation at the point r/d = 0.0 is 3%, while the maximum percentage deviation at the point r/d = 1.25 is 9.9%.

Inspection of the tables in appendix 2, shows that by increasing the distance from the nozzle axis, the maximum percentage deviation from the average is increased, and by decreasing the velocity, the maximum percentage deviation from the average is increased.

This deviation is due to the vortices initiated by the jet velocity inside the tank. So, extreme care was taken during the experiments to get accurate readings and to use the average value from the three different experiments for each Reynolds number.

CHAPTER 3

ANALYTICAL SOLUTION FOR SUBMERGED JETS

3.1 General

A submerged jet issuing from an orifice has a uniform starting velocity profile. For such jets, there are three main regions, see Fig.(5), for turbulent jet.

The initial region has a mixing boundary layer on the outside and a potential core along the axis in which the velocity remains constant. This is followed by a developing region where the axis velocity decreases with the distance from the nozzle, the velocity profile changes from the original shape and tends to become geometrically similar. In the fully developed region the profiles are similar and the axis velocity decays inversely with the distance from the nozzle.

For a jet issuing from a nozzle or a pipe where the flow is partially or fully developed, the three regions can not be clearly separated. Previous studies {1} with low Reynolds number jets (Re < 300) having parabolic starting profiles confirm that the axis velocity starts to decay at the nozzle exit and the flow becomes fully developed at about $\frac{x}{d} = 20$.

Classical solutions based on the assumption of profile similarity and a value of the virtual origin given by $\frac{x_o}{d} = 0.005\ Re$ give reasonable predictions for $\frac{x}{d} > 9$ but inaccurate for $1 < \frac{x}{d} < 9$.

For turbulent jets the fully developed starting profiles are more uniform and a core region exists. The core region occupies approximately the first 4 to 8 nozzle widths, depending on the shape of the starting profile, the degree of turbulence of the flow and also slightly on the shape of the nozzle.

Abramovich [2] uses a jet structure coefficient, α, to determine the core length, x, from the empirical expression

$$\frac{\alpha x}{d} = 0.67$$

Typical values of α are 0.076 to 0.066 for turbulent flows which give corresponding core lengths of $\frac{x}{d}$ = 4.4 to 5.0.

Beyond the initial region the jet axis velocity decays hyperbolically with the distance from some virtual origin and the jet width increases linearly with this distance.

The following section compares measured velocity distributions beyond the core region with classical solutions which are based on the assumption that the velocity at different locations are geometrically similar. This condition is usually only satisfied in the fully developed region ($\frac{x}{d}$ >20) and the purpose of the present study is to determine the limitations on these solutions in the region between the initial and fully developed regions.

Classical solutions in the initial region apply to jets issuing from orifices where the starting profile is uniform.

In this study the starting profile is fully developed and it is expected that the velocities will differ from the classical boundary layer solutions. The present study is therefore confined to comparing the measured profiles with existing solutions in the region $\frac{x}{d} > 4$ to 6.

3.2 Schlichting's solution {1}

Schlichting's solution for free turbulent jets is based on Prandtl's hypothesis for shearing stress.

This method can be applied only for the fully developed (main) region of the jet.

The width of the jet is proportional to x and the center-line velocity is inversely proportional to x, thus the virtual kinematic viscosity becomes:

$$\varepsilon_0 = \text{constant}$$

This means that ε_0 remains constant throughout the jet. The differential equation for the velocity distribution is identical with that for the Laminar jet, and the kinematic viscosity ν of Laminar flow is replaced by the virtual kinematic viscosity ε_0 of turbulent flow.

It is therefore possible to carry over the solution of the laminar jet case.

The classical similarity solution for the velocity component u becomes:

$$u = \frac{3}{8\Pi} \frac{J/\rho}{\varepsilon_o x'} \frac{1}{(1 + 0.25\ \eta^2)^2} \qquad (3.2.1)$$

where:

$$X' = X + X_o \qquad (3.2.2)$$

$$\eta = \frac{1}{4} \sqrt{\frac{3}{\Pi}} \frac{\sqrt{J/\rho}}{\varepsilon_o} \frac{r}{X} \qquad (3.2.3)$$

$\frac{\sqrt{J/\rho}}{\varepsilon_o}$ is an empirical constant.

According to the measurements performed by H. Reichardt the width of the jet is given by:

$$b_{.5} = 0.0848\ X \qquad (3.2.4)$$

where $b_{.5}$ is the half-width at half-depth.

Also, we have

$$b = 5.27\ x\ \frac{\varepsilon_o}{\sqrt{J/\rho}} \qquad (3.2.5)$$

Hence; the empirical constant $\frac{\varepsilon_o}{\sqrt{J/\rho}} = k = 0.0161$

The constant momentum flux of the jet in X direction is given by:

$$J = 2\rho\Pi \int_0^R u^2\ r dr \qquad (3.2.6)$$

The linear momentum flux at the nozzle exit in the X direction is:

$$J = U^2 \rho \frac{\Pi}{4} d^2 \qquad (3.2.7)$$

The velocity varies over the section, then the true average flux of momentum is

$$J = \beta\rho\, U_m^2\, \frac{\pi}{4}\, d^2 \qquad (3.2.8)$$

The momentum correction factor $\beta = 1.03 - 1.04$ for turbulent flow, and $\beta = 1.33$ for fully developed Laminar flow {3}.

The velocity profile at the nozzle exit (turbulent pipe flow {1} can be represented by the empirical equations

$$\frac{u}{U_o} = \left(\frac{r}{R}\right)^{1/n} \qquad (3.2.9)$$

$$\frac{u_m}{U_o} = \frac{2n^2}{(n+1)(2n+1)} \qquad (3.2.10)$$

where n varies with Reynolds number

The value of the exponent $n = 6$ is used to calculate the mean velocity at the nozzle exit at Re = 2937.

At Re = 1072. The mean exit velocity is assumed to be 60 percent of the maximum exit velocity.

The value of the momentum correction factor is assumed to be 1.04.

SAMPLE CALCULATIONS WITH $x_o = 0$. (Ideal virtual origin)

1. Re = 1072

U = 6.93 ft./sec.

ρ = 1.67066 lb.sec^2/ft.^{4}

d = 0.824 in.

Equation (3.2.8)

$$J = 1.04\ (1.67066)\ \{0.6 \times 6.93\}^2\ \frac{\pi}{4}\ \left(\frac{0.824}{12}\right)^2$$

$$= 0.111 \text{ lb.}$$

$$\varepsilon_o = 0.0161\ (0.111 \quad /1.67066)^{0.5}$$

$$= 0.00416 \text{ ft.}^2\text{/sec.}$$

Axis velocity

x/d = 12 x = 0.824 ft. (Equation (3.2.2))

Equation (3.3.1)

$$u = \frac{3}{8\pi}\ \frac{0.111}{0.00416\ (0.824)}\ /1.67066$$

u = 2.3187 ft./sec.

Jet spreading:

r/d = 1.213592 r = 0.0833 ft.

Equation (3.2.2)

$$\eta = \frac{1}{4} \sqrt{\frac{3}{\pi}} \times \frac{1}{0.0161} \times \frac{0.0833}{0.824}$$

$$= 1.5345$$

Equation (3.3.1)

$$u = \frac{3}{8\pi}\ \frac{0.111}{0.00416\ (0.824)}\ /1.67066\ \frac{1}{(1+0.25\ (1.5345\quad)^2)^2}$$

$$= 0.9186 \text{ ft./sec.}$$

2. $R_e = 2937$

$U_o = 18.99$ ft./sec.

$\rho = 1.670\ 66$ lb sec ^{2}/ft.^{4}

$n = 6$

$d = 0.824$ in.

Equation (3.2.10):

$$\frac{U_m}{U_o} = \frac{2\ (36)}{(6+1)\ (12+1)} = 0.79121$$

Equation (3.2.8)

$$J = 1.04\ (1.67066\ (18.99 \times 0.79121)^2 \frac{\pi}{4}\ \frac{(0.824)^2}{12}$$

$$= 1.4525 \quad \text{lb.}$$

Axis velocity:

$$\epsilon_o = 0.0161\ (1.4525\ /1.67066)^{0.5}$$

$$= 0.0150 \quad \text{ft}^2/\text{sec.}$$

Equation (3.3.1)

$$u = \frac{3}{8\pi}\ \frac{1.4525\ /1.67066}{0.0150\ X}$$

$$= \frac{6.9134}{X^1}$$

at $\frac{X}{d} = 12$; $x = 0.824$ Equation (3.2.2)

$$u = \frac{6.9134}{0.824}$$

$$= 8.390 \quad \text{ft./sec.}$$

Jet spreading

Equation (3.2.3)

$$\eta = \frac{1}{4} \times \frac{3}{\Pi} \times \frac{1}{0.0161} \times \frac{r}{x}$$

$$= 15.1739 \quad \frac{r}{x_1}$$

$x/d = 12 \qquad x = 0.824$ ft. Equation (3.2.2)

$$\eta = 18.4150 \quad r$$

$r/d = 1.2135 \qquad r = 1.0$ in. $= 0.0833$ ft.

Equation (3.3.1)

$$u = \frac{3}{8\Pi} \quad \frac{1.4525}{0.0150} \quad \frac{/1.67066}{(0.824)} \quad \frac{1}{(1+0.25\ (18.4150\quad)^2)^2}$$

$$= \frac{8.390}{(1+0.25\ (18.4150\quad X\ 0.0833\ )^2\ 1^2}$$

$$= 3.324 \text{ ft./sec.}$$

3.3 Abramovich's solution {2}

This method has two separate solutions for the initial and the main regions of the turbulent jets.

The initial region:

The center-line velocity in this region is considered to be constant and equal to the exit center-line velocity of the jet.

The boundary layer velocity profile is given by:

$$\frac{u}{U_o} = 2\eta^{1.5} - \eta^3 \qquad (3.3.1)$$

where

$$\eta = \frac{r - y_2}{y_1 - y_2} \qquad (3.3.2)$$

$$y_1 = R\left(0.112\left(\frac{X + X_{oh}}{R}\right) + 0.0015\left(\frac{X + X_{oh}}{R}\right)^2\right. \qquad (3.3.3)$$

$$\frac{y_1 - y_2}{X + X_{oh}} = 0.27 \qquad (3.3.4)$$

The meaning of each symbol is defined in the nomenclature.

The values of X_{oh} , X_h and x are given in graphs as functions of the boundary layer thickness.

The Main Region:

The axial velocity in the down-stream part of a round jet is given by:

$$\frac{U_{max}}{U_o} = 0.96/\frac{\alpha\, x'}{R} \qquad (3.3.5)$$

where

$$x' = x + x_o$$

$$\alpha = 0.076$$

For an equilibrium turbulent velocity field.

The location of the pole of the main region inside the nozzle is at a dimensionless distance from the exit equal to

$$\frac{\alpha\, x_o}{R} = 0.29 \qquad (3.3.6)$$

The velocity components at different points of the transverse cross section is given by:

$$\frac{u}{U_{max}} = \frac{z' e^{z}}{\phi} \qquad (3.3.7)$$

where

$$\phi = \frac{r}{\alpha\, x} \qquad (3.3.8)$$

and

$$z' = 0.25\,(3.4-\phi)^2 - 0.037\,(3.4-\phi)^3 - 0.004\,(3.4-\phi)^4 - 0.015\,(3.4-\phi)^5 - 0.0173\,(3.4-\phi)^6 + \qquad (3.3.9)$$

This main region begins at a distance equal to X_n from the nozzle exit.

Equation (3.3.7) is given in tabulated form.

Sample calculations

Initial Region:

axis velocity: $\frac{U_{max}}{U_o} = 1$

jet spreading:

station $\frac{X}{d} = 1$ $\quad X = \frac{0.824}{12} = 0.0686$ ft.

r = 0.0 ft. w.r.t. tube surface

r = 0.03433 ft. w.r.t. center-line

$x_{oh} = 0.0686$ ft.

Equation (2.3.3)

$$y_1 = 0.03433 \left(0.112 \left(\frac{0.0686 + 0.0686}{0.03433}\right) + 0.0015 \left(\frac{0.0686 + 0.0686}{0.03433}\right)^2\right)$$

$$= 0.0162 \text{ ft.}$$

Equation (3.3.4):

$$y_2 = 0.0162 - 0.27 (0.0686 + 0.0686)$$

$$= -0.02087 \text{ ft.}$$

Equation (3.3.2):

$$\eta = \frac{0.0 + 0.02087}{0.0162 + 0.02087}$$

$$= 0.5629$$

Equation (3.3.1):

$$\frac{u}{U_o} = 2 (0.5629)^{1.5} - (0.6296)^3$$

$$= 0.666$$

Main Region:

begins at $\frac{X_n}{d} = 3.1$

Equation (3.3.5):

$$\frac{U_{max}}{U_o} = \frac{0.96\ (0.824)}{0.076\ (2)\ (12)\ X}$$

$$= \frac{0.433}{X}$$

Equation (3.3.6):

$$x_o = 0.29\ \frac{(0.824)}{12\ (2)\ (0.076)}$$

$$= 0.131 \text{ ft.}$$

For $\frac{X}{d} = 12$ $\quad X = 0.824$ ft.

$\frac{X}{d} = 12 + 3.1 = 15.1$ $\quad$ actual X = 0.824 + 0.131 ft.

$$\frac{U_{max}}{U_o} = \frac{0.433}{(0.824+0.131)} = 0.4541$$

For $\frac{r}{d} = 1.2849$ $\quad r = 0.0882$ $\quad$ ft.

Equation (3.3.8):

$$\phi = \frac{0.0882}{0.076\ (1.03+0.131)}$$

$$= 1.0$$

From table, $\frac{u}{U_{max}} = 0.606$

DISCUSSION OF RESULTS

Fig. (6) through (14) and (15) through (23) show typical velocity profiles obtained experimentally and analytically for the jet center-line exit velocities of 18.99 and 6.93 f.p.s. respectively (Re = 2937, 1072).

Schlichting's analytical results are referred to as "the ideal virtual origin", (equations (3.2.1) to (3.2.8) assuming $X_o = 0$)

"The modified virtual origin", refers to equations (3.2.1) to (3.2.8) in which the virtual origin has been adjusted ($\frac{X_o}{d}$ = 4.7 for Re = 2937 and $\frac{X_o}{d}$ = 9 for Re = 1072) to get the best agreement with the experimental results.

Center-Line Velocity decay:

Inspection of Figs. (14) and (23) show the ideal virtual origin does not give a good velocity prediction for the center-line velocities while the calculated values are too low.

By adjusting the virtual origin, better agreement cannot be obtained except in the outer region where X/d > 21. In this region the calculated values are very near to the experimental values, i.e. the modified virtual origin theory gives good velocity prediction for the center-line velocity decay in the outer region where X/d > 21.

Abramovich's solution does not represent the center-line velocity decay in the initial region of the jet. In the main region the method does not represent the velocity prediction up to an axial distance equal to 18 jet diameters. In the region where X/d > 18 Abramovich's solution has values very near to the experimental values.

Jet Spreading:

Equation (3.2.4) represents Schlichting's solution for the half-width at half-depth.

Figs. (24) and (25) represent Schlichting's solution, assuming different values for the empirical constant as well as the experimental representation for the half-width at half-depth.

The inspection of figs. (24) and (25) shows that Schlichting's solution does not represent the experimental values for the half-width at half-depth.

By adjusting the value of the empirical constant k in equation (3.2.3), better agreement with measurements is obtained. The adjusted values are 0.0131 and 0.0095 for Reynolds numbers equal to 2937 and 1072 respectively.

By increasing the value of the empirical constant, the slope of the theoretical solution is increased.

Abramovich's solution does not give a good representation for the half-width at half-depth as the calculated values are too high.

Velocity profile development:

Inspection of Figs. (6) through (13) and (15) through (22) show that for the near region of the jet, where $X/d < 21$, neither the virtual origin theory nor the modified virtual origin represents the velocity predictions.

For the far region, where $X/d > 21$, the modified virtual origin gives good velocity predictions in the central jet region ($o < r/d < 1.5$), but in the outer region ($r/d > 1.5$) the method does not give good velocity predictions where the calculated values are too high.

In this far region ($X/d > 21$), the modified virtual origin theory gives reasonable agreement with the measurements up to $r/d = 1.5$, if the origin is taken at $X/d = 4.7$ inside the nozzle for Reynolds number = 2937, and at $X/d = 9$ inside the nozzle for Reynolds number = 1072.

Figs. (20) to (27) show the similarity parameter η (Equation (3.2.3)) using these adjusted values for the virtual origin for the two values of Reynolds numbers of 2937 and 1072, respectively. It is clear that the profiles in each case are similar.

In the near region of the jet where $X/d < 18$, Abramovich's solution does not give good velocity prediction, while the calculated values are too high in all the central region of the jet.

In the far region where $X/d > 18$, Abramovich's solution gives good velocity predictions for the central jet region ($o < r < 0.45$) while in the outer region where $r/d > 0.45$, the method does not represent the measured values where the calculated values are too high.

Fig. (28) shows the effect of the momentum correction factor on Schlichting's solution for Re = 1072 at the station $X/d = 6$. By increasing the value of the momentum correction factor from 1.04 to 1.33, the dimensionless axisymmetric jet velocity is slightly increased.

3.4 Comparison with Results reported by Hinze (Ref.{15}p. 538)

Because of the poor agreement with the solutions of Schlichting and Abramovich, an attempt is made to obtain the optimum values of the virtual origin x_o and ε_o using Hinze's solution which is based on a constant value of the kinematic viscosity.

$$\varepsilon_o = C_1 (x + x_o) U_{max} \qquad (3.4.1)$$

The velocity profiles are given by

$$\frac{u}{U_{max}} = \frac{1}{(1+ \frac{1}{8C_1} \eta^2)^2} \qquad (3.4.2)$$

where $C_1 = 0.00196$ for fully turbulent jet and

$$\eta = \frac{r}{x+x_o}$$

It is to be expected that C_1 will have a smaller value for semi-turbulent jets.

Axis Velocity Decay

Equations (3.4.1) and (3.4.2) require appropriate values of x_o. The expression for the hyperbolic axis velocity decay is:

$$\frac{u}{U_o} = F \frac{d}{x+x_o} \qquad (3.4.3)$$

where F = 5.4 to 5.9 based on experimental results with fully turbulent jets reported by Hinze.

The value of x_o depends on the initial velocity U_o The appropriate value of x_o for the present study is most conveniently obtained from the expression

$$\frac{U_o}{U_{max}} = \frac{1}{F}\frac{x}{d} + \frac{x_o}{Fd} \qquad (3.4.4)$$

Figure (30) is a plot of $\frac{U_o}{U_{max}}$ vs $\frac{x}{d}$ for the two Reynolds numbers.

A linear regression analysis of the experimental data for $6 < \frac{x}{d} < 24$ gives the following values

$$F = 7.14,\ \frac{x_o}{d} = 1.57 \text{ for } U_o = 6.93 \text{ f.p.s., Re=1072} \qquad (3.4.5a)$$

and $$F = 7.69,\ \frac{x_o}{d} = 2.31 \text{ for } U_o = 18.99 \text{ f.p.s., Re=2937} \qquad (3.4.5b)$$

The linear correlation coefficient in both cases is close to 1 thus indicating that the axis velocity decays almost exactly in accordance with the inverse of the distance from virtual origins located at $\frac{x_o}{d} = 1.57$ and $\frac{x_o}{d} = 2.31$ respectively.

Equation (3.4.4) with the appropriate values of 3.4.5(a) and (b) can be used to compare the present results with published data for laminar and turbulent jets.

The virtual origin

For laminar jets the expression for the virtual origin is

$$\frac{x_o}{d} = 0.055\ Re \qquad (3.4.6)$$

and for turbulent jets experimentally determined values differ widely from $\frac{x_o}{d} = -0.5$ to $\frac{x_o}{d} = -3$

Equation (3.4.4) with the appropriate statistical values given in (3.4.5) of the coefficients give the following expression for equation (3.4.6).

$$\frac{x_o}{d} = 0.00146\ Re \qquad (3.4.6a)$$

and $$\frac{x_o}{d} = 0.00078\ Re \qquad (3.4.6b)$$

This indicates that the virtual origin is much less dependent on Reynolds number in the semi-turbulent region, but that it still retains the laminar characteristics that $\frac{x_o}{d} > 0$.

The Potential Core

The experimental data show that the axis velocities start to decay at $3 < \frac{x_o}{d} < 6$, Equations 3.4.4 and 3.4.5 (a) and (b) can be used to give statistical values for the apparent lengths of the potential core x_h where $U = U_o$. As expected the calculated values of $\frac{x_h}{d} = 5.59$ and 5.44 are slightly below the range of 6 to 9 reported by Hinze for turbulent jets.

Velocity Profiles

Measured velocity profiles can be compared with the solution of equation (3.4.2) using values of x_o obtained from the linear regression equation (3.4.4). The optimum experimental value of C_1 in equation (3.4.1) is obtained at the half velocity width for each location from the nozzle. At this location $\frac{u}{U_{max}} = 0.5$ and equation (3.4.2) yields the following relationship between C_1 and the half-velocity width, $b_{0.5}$

$$C_1 = 0.302\ \eta_{0.5}^2$$

where $\eta_{0.5} = \frac{b_{0.5}}{X + X_o}$

The values of $\eta_{0.5}$ are obtained from the slopes of plots of $b_{0.5}$ vs x (or $x + x_o$) as shown in figures (24) and (25) for the two jet velocities.

For Re = 2937 : $\eta_{0.5} = 0.068$, $C_1 = 0.00139$

For Re = 1072 : $\eta_{0.5} = 0.0488$, $C_1 = 0.00072$

with these values of C_1 equation (3.4.2), becomes

For Re = 2937; $\frac{u}{U_{max}} = \frac{1}{(1 + 89.93\,\eta^2)^2}$ with $\eta = \frac{r}{X+2.31}$ (3.4.2a)

For Re = 1072; $\frac{u}{U_{max}} = \frac{1}{(1 + 173.6\,\eta^2)^2}$ with $\eta = \frac{r}{X+1.57}$ (3.4.2b)

Numerical values of equations 3.4.2a and b are listed with experimental values in tables 5 and 6 and are also plotted in Figures (31) and (32).

The figures show that the experimental results tend to fall below the theoretical curve. The best agreement is in the central jet region ($0 < \eta < 0.06$). For all distances from the nozzle. The optimized values of X_o and ε_o give the best agreement with experimental profiles taken at distance midway between the core and fully-developed regions.

For Re = 2937 there is almost perfect agreement at $\frac{x}{d} = 15$

CONCLUSION

The experimental results of this study for jet Reynolds numbers of 2937 and 1072 show that near to the jet exit. neither Schlichting's solution with the ideal virtual origin nor Schlichting's solution with the modified virtual origin predict the velocity decay in the region where $x/d < 21$.

Schlichting's solution can be applied to regions greater than 21 nozzle diameters from the exit and for the central region of ($o < r/d < 1.5$) if the virtual origin is taken at $x/d = 4.7$, $x/d = 9$ for Reynolds numbers of 2937 and 1072, respectively.

Abramovich's solution does not predict the axial velocity decay except in the region where $x/d > 18$ from the nozzle exit. In this region the method represents the velocity decay in the transverse direction up to $r/d = 0.45$.

Neither Schlichting's solution for turbulent jets nor Abramovich's solution for turbulent jets represent the complete solution for the semi-turbulent jets.

Hinze's solution with optimized values of x_o and ε_o gives reasonable predictions in the central jet region at all locations where $6 < \frac{x}{d} < 24$. In the outer jet regions, Hinze's solution gives velocities higher than the measure values.

This study emphasizes the limitations of existing closed-form solutions for semi-turbulent flows in the near region of the nozzle.

REFERENCES

1. Schlichting, H., "Boundary Layer Theory", McGraw-Hill, 6th edition, 1968, pp. 560-563, pp. 681-700.

2. Abramovich, G.N., "Theory of Turbulent Jets", M.I.T. Press, Cambridge, Mass., 1963, pp. 76-84, pp. 505-512.

3. Harleman, R.F. and Daily, M.W., "Fluid Dynamics", Addison-Wesley Publishing Company, Inc., Mass., 1966.

4. Tsang, S.H.L., "A Study of Axisymmetric Submerged Jets Relevant to Turbulent Amplifier Design", Master Thesis, Department of Mechanical Engineers, Sir George Williams University, Montreal, Canada, August 1971.

5. duPlessis, M.P., Wang, R.L. and Tsang, S., "Development of Submerged Round Laminar Jet from an Initially Parabolic Profile", an ASME Transaction, Journal of System Dynamics, Measurement and Control, Vol. 95, Series G, No. 2, pp. 148-154, June 1973.

6. duPlessis, M.P. and Wang, R.L., "An Explicit Numerical Method for the Solution of Jet Flows", an ASME Transaction, Journal of Fluids Engineering, Vol. 95, Series I, No. 1, pp. 38-46, March 1973.

7. Prandtl, L.O. Tietjens, "Fundamentals of Hydro-and-Aero-Mechanics", New York (1934).

8. Andrade, E.N. da C. and Tsien, L.C., "The Velocity Distribution in a Liquid into Liquid Jet", Phys. Soc., Vol. 49, pt., 4, pp. 381-391, 1937.

9. Reynolds, A.J., "Observations of a Liquid into Liquid Jet", J.F.M. 14, pp. 552-556, 1962.

10. Domm, V., Fabian, H., Wehrmann, O. and Wille, R., "Contributions on the Mechanics of Laminar-Turbulent Transaction of Jet Flow", Air Force Office of Sci. Res. Agency (ASTIA) Document, No. AD 820004, 1955.

11. McNaughton, K.J. and Sinclair, C.G., "Submerged Jets in Short Cylindrical Flow Vessels", J.F.M. 25, pp. 367-375, 1966.

12. Bickley, W., "The Plane Jet, Philosophical Magazine, Vol. 7, 1937, p. 156.

13. Schlichtin, H., "Laminar Strachlausberiehung", ZAMM, Bd. 13, 1933, pp. 260-263.

14. Nikuradse, J., "Gesetzmassigkeit der Burbulenten Stromung in Glutten Rohren", Forsch. Arb., Ing. West, No. 356 (1932).

15. Hinze, J.O., "Turbulence", McGraw-Hill Book Company, 2nd Edition, 1975.

APPENDIX I

Table I

EXPERIMENTAL DATA

r inch		0.000	0.125	0.250	0.375	0.500	0.625	0.750	0.875	1.000	1.125	1.250	1.375	1.500	1.625	1.750
x/d	Exp. No.	local velocity - Fps.														
1	1	6.930	6.463	4.691	1.906	0.289	0.020	0.017	0.015	0.013	0.006	0.006	0.005	0.005	0.065	0.005
	2	6.930	6.625	4.277	1.799	0.259	0.029	0.018	0.020	0.017	0.015	0.015	0.014	0.011	0.008	0.005
	3	6.930	6.253	4.550	1.911	0.283	0.025	0.019	0.019	0.009	0.018	0.018	0.015	0.008	0.005	0.008
	aver.	6.930	6.447	4.506	1.872	0.277	0.023	0.018	0.018	0.013	0.013	0.013	0.013	0.009	0.005	0.005
3	1	6.755	6.215	4.279	2.092	0.605	0.149	0.025	0.007	0.005	0.005	0.005	0.005	0.005	0.005	0.005
	2	6.921	6.301	4.660	2.029	0.632	0.127	0.026	0.008	0.005	0.005	0.005	0.005	0.005	0.005	0.005
	3	6.907	6.201	4.579	2.431	0.635	0.141	0.018	0.012	0.005	0.005	0.005	0.005	0.005	0.005	0.005
	aver.	6.897	6.239	4.506	2.184	0.624	0.139	0.023	0.009	0.005	0.005	0.005	0.005	0.005	0.005	0.005
6	1	6.202	5.810	4.401	2.371	0.911	0.421	0.143	0.036	0.011	0.005	0.005	0.005	0.005	0.005	0.005
	2	6.015	5.699	4.313	2.239	1.037	0.398	0.141	0.042	0.018	0.005	0.005	0.005	0.005	0.005	0.005
	3	6.284	5.543	4.276	2.254	0.965	0.429	0.133	0.045	0.010	0.005	0.005	0.005	0.005	0.005	0.005
	aver.	6.169	5.684	4.330	2.288	0.971	0.416	0.139	0.041	0.013	0.005	0.005	0.005	0.005	0.005	0.005
12	1	3.850	3.630	3.151	2.130	1.072	0.425	0.142	0.098	0.075	0.071	0.005	0.005	0.005	0.005	0.005
	2	3.689	3.651	3.220	2.279	1.122	0.420	0.129	0.118	0.071	0.067	0.005	0.005	0.005	0.005	0.005
	3	3.687	3.429	2.986	2.662	1.238	0.403	0.135	0.096	0.061	0.066	0.005	0.005	0.005	0.005	0.005
	aver.	3.742	3.570	3.119	2.357	1.144	0.416	0.139	0.104	0.069	0.066	0.005	0.005	0.005	0.005	0.005

U_o = 6.93 f.p.s.

Table I (cont'd)

EXPERIMENTAL DATA

r inch		0.000	0.125	0.250	0.375	0.500	0.625	0.750	0.875	1.000	1.125	1.250	1.375	1.500	1.625	1.750
x/d	Exp. No.	local velocity - Eps.														
15	1	3.201	3.027	2.466	2.315	1.390	0.925	0.491	0.290	0.142	0.069	0.060	0.026	0.016	0.017	0.014
	2	3.131	2.960	2.413	2.374	1.501	1.022	0.455	0.271	0.131	0.073	0.058	0.020	0.020	0.010	0.015
	3	2.713	2.851	2.192	2.175	1.579	0.756	0.509	0.270	0.120	0.077	0.056	0.023	0.018	0.012	0.010
	aver.	3.050	2.946	2.357	2.288	1.490	0.901	0.485	0.277	0.137	0.073	0.061	0.023	0.018	0.013	0.013
18	1	2.608	2.458	2.307	2.010	1.819	1.687	1.362	1.039	0.670	0.486	0.378	0.247	0.107	0.076	0.073
	2	2.429	2.400	2.379	2.221	1.993	1.623	1.391	1.018	0.691	0.498	0.362	0.221	0.110	0.070	0.063
	3	2.655	2.525	2.301	2.216	2.011	1.682	1.303	0.958	0.613	0.471	0.301	0.261	0.105	0.062	0.071
	aver.	2.599	2.461	2.329	2.149	1.941	1.664	1.352	1.005	0.658	0.485	0.347	0.243	0.104	0.069	0.069
21	1	2.127	2.022	1.989	1.921	1.724	1.599	1.321	1.156	0.938	0.759	0.553	0.427	0.343	0.194	0.135
	2	2.345	2.261	2.202	2.121	1.866	1.590	1.417	1.100	0.981	0.730	0.522	0.365	0.299	0.299	0.103
	3	2.182	2.164	2.151	1.988	1.921	1.698	1.318	1.278	0.889	0.695	0.590	0.351	0.294	0.221	0.095
	aver.	2.218	2.149	2.114	2.010	1.837	1.629	1.352	1.178	0.936	0.728	0.555	0.381	0.312	0.208	0.111
24	1	1.713	1.805	1.769	1.620	1.590	1.572	1.330	1.088	0.921	0.801	0.616	0.541	0.441	0.332	0.283
	2	1.865	1.859	1.835	1.806	1.633	1.495	1.371	1.200	1.107	0.851	0.666	0.523	0.418	0.298	0.257
	3	1.925	1.952	1.802	1.773	1.664	1.508	1.355	1.246	1.071	0.844	0.695	0.601	0.389	0.306	0.281
	aver.	1.901	1.872	1.802	1.733	1.629	1.525	1.352	1.178	1.033	0.832	0.659	0.555	0.416	0.312	0.27

U_o = 6.93 f.p.s.

Table 2

EXPERIMENTAL DATA

r inch		0.004	0.125	0.250	0.375	0.500	0.625	0.750	0.875	1.000	1.125	1.250	1.375	1.500	1.625	1.750
x/d	Exp. No.	local velocity - Fps.														
1	1	18.990	17.990	16.929	5.081	0.483	0.201	0.188	0.190	0.190	0.180	0.155	0.128	0.125	0.120	0.118
	2	18.990	18.022	16.201	5.410	0.505	0.188	0.195	0.185	0.171	0.147	0.140	0.136	0.130	0.119	0.112
	3	18.990	18.138	17.030	5.469	0.437	0.181	0.187	0.180	0.170	0.168	0.158	0.138	0.135	0.130	0.115
	aver	18.990	18.050	16.720	5.320	0.475	0.190	0.190	0.185	0.177	0.165	0.151	0.134	0.130	0.123	0.115
3	1	18.980	17.711	13.925	6.887	0.895	0.450	0.375	0.389	0.374	0.338	0.292	0.292	0.279	0.264	0.229
	2	18.990	17.250	14.500	6.904	0.811	0.498	0.355	0.355	0.340	0.331	0.300	0.294	0.283	0.277	0.201
	3	19.00	16.624	14.398	7.014	0.859	0.477	0.410	0.405	0.396	0.390	0.368	0.338	0.329	0.329	0.224
	aver	18.990	17.195	14.250	6.935	0.855	0.475	0.380	0.380	0.370	0.353	0.320	0.308	0.297	0.269	0.218
6	1	17.303	15.201	13.413	8.997	6.001	3.195	1.982	1.661	1.216	0.787	0.509	0.450	0.403	0.301	0.186
	2	16.982	14.983	13.020	9.301	6.324	3.475	2.213	1.950	1.360	0.901	0.598	0.502	0.362	0.292	0.205
	3	17.015	14.846	12.897	9.347	6.485	3.890	2.360	1.804	1.229	0.87	0.603	0.473	0.375	0.262	0.179
	aver	17.100	15.010	13.110	9.215	6.270	3.420	2.185	1.805	1.235	0.855	0.570	0.475	0.380	0.285	0.190
12	1	10.001	9.350	9.351	9.154	7.987	7.761	7.363	5.208	4.103	3.821	3.355	2.286	1.501	1.340	1.161
	2.	9.853	9.632	8.927	8.799	7.252	7.095	6.988	5.911	3.820	3.268	2.982	1.998	1.630	1.528	1.088
	3	9.501	9.518	9.367	9.122	7.561	7.574	7.307	5.511	4.074	4.026	3.353	2.556	1.716	1.407	1.171
	aver	9.785	9.500	9.215	9.025	7.600	7.410	7.220	5.510	3.990	3.705	3.230	2.280	1.615	1.425	1.140

U_o = 18.99 f.p.s.

Table 2 (cont'd)

EXPERIMENTAL DATA

r inch		0.000	0.125	0.250	0.375	0.500	0.625	0.750	0.875	1.000	1.125	1.250	1.375	1.500	1.625	1.750
x/d	Exp. No.	Local velocity - Fps.														
15	1	8.021	7.977	7.785	7.785	6.921	6.278	5.401	5.101	3.021	4.242	3.001	2.565	2.201	1.730	1.525
	2	8.971	7.820	7.310	7.102	6.205	5.611	5.057	4.431	2.554	2.500	2.718	2.523	1.889	1.699	1.398
	3	8.088	8.478	7.705	7.628	6.824	6.351	5.217	5.003	2.975	2.948	2.836	2.322	1.895	1.701	1.352
	aver.	8.360	8.075	7.600	7.505	6.650	6.080	5.225	4.845	2.850	3.230	2.945	2.470	1.995	1.710	1.425
18	1	7.259	7.119	6.846	6.110	5.814	5.169	4.585	4.086	3.620	2.764	2.213	2.015	1.664	1.520	1.277
	2	6.890	6.491	6.198	5.809	5.102	4.871	4.124	3.673	3.528	2.981	2.872	2.448	2.216	1.925	1.785
	3	7.226	7.195	6.621	6.321	5.899	5.350	4.686	4.211	3.112	3.378	2.890	2.380	2.105	1.856	1.498
	aver.	7.125	6.935	6.555	6.080	5.605	5.130	4.465	3.990	3.420	3.041	2.660	2.281	1.995	1.767	1.520
21	1	6.602	6.528	6.246	5.312	5.201	4.981	4.594	4.213	3.821	3.221	3.180	2.352	2.201	1.844	1.285
	2	5.972	5.790	5.581	5.220	5.182	4.227	4.165	3.875	3.392	3.078	2.883	2.331	2.091	1.879	1.505
	3	6.239	6.207	6.128	5.713	5.577	4.757	4.354	4.167	3.044	2.821	2.202	2.157	1.981	1.692	1.485
	aver.	6.271	6.175	5.985	5.415	5.320	4.655	4.371	4.085	3.419	3.040	2.755	2.280	2.091	1.805	1.425
24	1	5.184	4.912	4.582	5.105	5.081	4.891	4.238	4.118	3.803	3.621	2.481	2.241	1.991	1.573	1.520
	2	5.301	5.248	5.125	5.065	4.764	4.471	3.933	3.871	3.549	3.208	2.763	2.683	2.081	1.812	1.658
	3	5.478	5.230	4.728	4.553	4.411	4.321	4.078	3.981	3.481	3.821	3.021	2.771	2.201	2.030	1.667
	aver.	5.321	5.130	4.845	4.941	4.752	4.561	3.993	3.990	3.611	3.420	2.755	2.565	2.091	1.805	1.615

U_o = 18.99 f.p.s

APPENDIX 2

Table 3

PERCENTAGE DEVIATION - EXPERIMENTAL DATA

inch		0.000	0.125	0.250	0.375	0.500	0.625	0.750	0.875	1.000	1.125	1.350	1.375	1.500	1.625	1.750
x/d		Average velocities f.p.s. - and - maximum % deviation from the average														
1	aver	6.930	6.447	4.506	1.872	0.277	0.023	0.018	0.018	0.013	0.013	0.013	0.013	0.009	0.005	0.005
	% dev.	0.0	3.0	5.1	3.9	6.5	2.6	5.5	16.6	30.7	38.5	38.5	61.5	44.4	60.0	00.0
3	aver	6.897	6.239	4.506	2.184	0.624	0.139	0.023	0.009	0.005	0.005	0.005	0.005	0.005	0.005	0.005
	% dev.	2.1	9.9	5.0	11.3	3.0	8.6	21.7	33.3	0.0	0.0	0.0	0.0	0.0	0.0	0.0
6	aver	6.159	5.684	4.330	2.228	0.971	0.416	0.139	0.041	0.013	0.005	0.005	0.005	0.005	0.005	0.005
	% dev.	2.5	.5	1.6	3.6	6.8	4.3	4.3	12.2	38.5	0.0	0.0	0.0	0.0	0.0	0.0
12	aver	3.742	3.570	3.119	2.357	1.144	0.416	0.139	0.104	0.069	0.066	0.005	0.005	0.005	0.005	0.005
	% dev.	2.9	4.0	4.3	12.9	8.2	3.1	7.2	13.5	11.6	7.6	0.0	0.0	0.0	0.0	0.0
15	aver	3.050	2.946	2.357	2.288	1.490	0.901	0.485	0.277	0.137	0.073	0.061	0.023	0.018	0.013	0.013
	% dev.	11.1	3.2	7.0	4.9	6.7	16.1	6.2	4.7	12.4	5.5	8.2	13.0	11.1	30.7	23.1
18	aver	2.599	2.461	2.329	2.149	1.941	1.664	1.352	1.005	0.658	0.485	0.347	0.243	0.104	0.069	0.069
	% dev.	6.5	2.6	2.2	6.5	6.3	2.5	3.6	4.7	6.8	3.7	13.3	9.1	3.9	10.1	8.7
21	aver	2.218	2.149	2.114	2.010	1.837	1.629	1.352	1.178	0.936	0.728	0.555	0.381	0.312	0.208	0.111
	% dev.	5.7	.9	5.9	5.5	6.2	4.2	4.8	8.5	5.0	4.5	12.1	12.1	9.9	4.8	21.6
24	aver	1.901	1.872	0.802	1.733	1.629	1.525	1.352	1.178	1.033	0.832	0.659	0.555	0.416	0.312	0.277
	% dev.	9.9	4.3	1.8	6.5	2.4	3.1	1.6	7.6	10.8	3.7	9.7	8.3	6.5	6.4	7.2

U_o = 6.93 f.p.s.

Table 4

ERCENTAGE DEVIATION - EXPERIMENTAL DATA

r inch		0.000	0.125	0.250	0.375	0.500	0.625	0.750	0.875	1.000	1.125	1.250	1.375	1.500	1.625	1.750
x/d		Average velocities f.p.s. - and - maximum % deviation from the average														
1	aver	18.990	18.050	16.720	5.320	0.475	0.190	0.190	1.185	0.177	0.165	0.151	0.134	0.130	0.123	0.115
	% dev.	0.0	0.5	3.1	4.5	8.0	5.7	2.6	2.7	7.3	10.0	7.2	4.4	3.8	5.6	2.6
3	aver	18.990	17.195	14.250	6.935	0.855	0.475	0.380	0.380	0.370	0.353	0.320	0.308	0.297	0.269	0.218
	% dev.	0.0	3.0	2.2	1.1	5.1	5.2	7.9	6.6	8.1	10.0	15.0	9.7	10.7	22.0	7.7
6	aver	17.100	15.010	13.110	9.215	6.270	3.420	2.185	1.805	1.235	0.855	0.570	0.475	0.380	0.285	0.190
	% dev.	1.1	1.1	2.3	2.4	4.2	13.7	9.3	8.0	10.0	8.0	10.7	5.7	6.0	8.1	7.9
12	aver	9.785	9.500	9.215	9.025	7.600	7.410	7.220	5.510	3.990	3.705	3.230	2.280	1.015	1.425	1.140
	% dev.	2.9	1.6	3.1	2.5	4.6	4.7	3.2	7.3	4.3	11.8	3.9	12.4	7.1	7.2	4.6
15	aver	8.360	8.075	7.600	7.505	6.650	6.080	5.225	4.845	2.850	3.230	2.945	2.470	1.995	1.710	1.425
	% dev.	7.3	5.0	3.8	5.4	6.7	7.7	3.4	8.6	10.4	31.3	7.7	6.0	10.3	1.2	7.0
18	aver	7.125	6.935	6.555	6.080	5.605	5.130	4.465	3.990	3.420	3.041	2.660	2.281	1.995	1.767	1.520
	% dev.	3.3	6.4	5.5	4.5	9.0	5.1	7.6	7.9	9.0	11.1	16.8	7.3	16.7	13.9	15.9
21	aver	6.271	6.175	5.985	5.415	5.320	4.655	4.371	4.085	3.419	3.040	2.755	2.280	2.091	1.805	1.425
	% dev.	5.3	6.2	6.8	5.5	4.8	9.2	5.1	5.1	11.8	7.2	20.0	5.4	5.3	6.3	9.8
24	aver	5.231	5.130	4.845	4.941	4.752	4.561	3.993	3.990	3.611	3.420	2.755	2.565	2.091	1.805	1.615
	% dev.	3.0	4.3	5.8	7.8	7.2	7.2	6.1	3.2	5.3	11.7	9.9	12.6	5.3	12.5	5.9

U_o = 18.99 f.p.s.

APPENDIX 3

TABLE 6

VELOCITY PROFILES

r inch		0.0	.125	.250	.375	.500	.625	.750	.875	1.0	1.125	1.250	1.375	1.500	1.625	1.750
Theoretical Results																
η		0.01	0.02	0.03	0.04	0.05	0.06	0.07	0.08	0.09	0.10	0.11	0.12	0.13	0.14	0.15
Ψ		0.966	0.874	0.748	0.613	0.486	0.379	0.292	0.224	0.173	0.134	0.104	0.082	0.065	0.052	0.042
x/d		Experimental Results														
1	η	0	.059	.118	.177	.236	.295	.354	.413	.472	.531	.590	.649	.708	.767	.826
	Ψ	1	0.930	0.650	0.270	0.040	0.003	0.003	0.003	0.002	0.002	0.002	0.002	0.001	0.001	0.001
6	η	0	.020	.040	.060	.080	.100	.120	.140	.160	.180	.200	.220	.240	.260	.280
	Ψ	1	0.921	0.702	0.371	0.157	0.067	0.023	0.007	0.002	0.001	0.001	0.001	0.001	0.001	0.001
12	η	0	.011	.022	.034	.045	.056	.067	.078	.089	.101	.112	.123	.134	.145	.157
	Ψ	1	0.943	0.834	0.630	0.306	0.111	0.037	0.028	0.018	0.018	0.001	0.001	0.001	0.001	0.001
15	η	0	.009	.018	.026	.035	.044	.055	.064	.073	.082	.092	.100	.110	.119	.128
	Ψ	1	0.966	0.773	0.750	0.489	0.295	0.159	0.091	0.045	0.024	0.02	0.008	0.006	0.004	0.004
21	η	0	.007	.013	.020	.027	.034	.040	.047	.054	.060	.067	.074	.081	.087	.094
	Ψ	1	0.969	0.953	0.906	0.828	0.735	0.610	0.531	0.422	0.328	0.250	0.172	0.141	0.094	0.050
24	η	0	.006	.012	.018	.024	.030	.035	.042	.047	.053	.059	.065	.071	.077	.083
	Ψ	1	0.985	0.948	0.912	0.857	0.802	0.711	0.620	0.543	0.438	0.347	0.292	0.219	0.164	0.146

U_o = 6.93 f.p.s., x_o/d = 1.57, $\Psi = u/U_{max}$

TABLE 5

VELOCITY PROFILES

r inch		00	0.125	0.250	0.375	0.500	0.625	0.725	0.875	1.000	1.125	1.250	1.375	1.500	1.625	1.750
Theoritical Results																
η		0.01	.02	.03	.04	.05	.06	.07	.08	.09	.10	.11	.12	.13	.14	.15
Ψ		0.982	.932	.856	.764	.667	.571	.482	.403	.335	.277	.229	0.190	.092	.131	.109
x/d		Experimental Results														
1	η	0	.046	.092	.137	.183	.229	.275	.321	.367	.412	.458	.504	.550	.596	.642
	Ψ	1	.951	.881	.280	.025	.010	.010	.009	.009	.0086	.0079	.001	.0068	.0065	.0061
6	η	0	.0183	.0365	.0548	.0730	.0913	.1095	.1278	.146	.1643	.1826	.2008	.219	.2373	.2556
	Ψ	1.0	.878	.767	.539	.367	.20	.128	.106	.072	.050	.033	.028	.022	.017	.011
12	η	0	0.011	.021	.032	.042	.053	.064	.074	.085	.095	.106	.117	.127	.138	.148
	Ψ	1	.971	.942	.922	.777	.757	.738	.563	.408	.379	.330	.233	.165	.146	.117
15	η	0	.009	.018	.026	.035	.044	.053	.061	.070	.0789	.088	.096	.105	.114	.123
	Ψ	1	.966	.909	.899	.795	.727	.625	.580	.341	.386	.352	.295	.239	.204	.170
21	η	0	.007	.013	.020	.026	.033	.039	.046	.052	.059	.065	.072	.078	.085	.091
	Ψ	1	.985	.954	.864	.848	.742	.697	.651	.545	.485	.439	.364	.333	.288	.227
24	η	0	.006	.012	.017	.023	.029	.035	.040	.046	.052	.058	.063	.069	.075	.081
	Ψ	1	.964	.911	.929	.893	.857	.750	.750	.678	.643	.518	.482	.393	.339	.304

$U_o = 18.99$, $\frac{X_o}{d} = 2.31$, $\Psi = \frac{u}{U_{max}}$

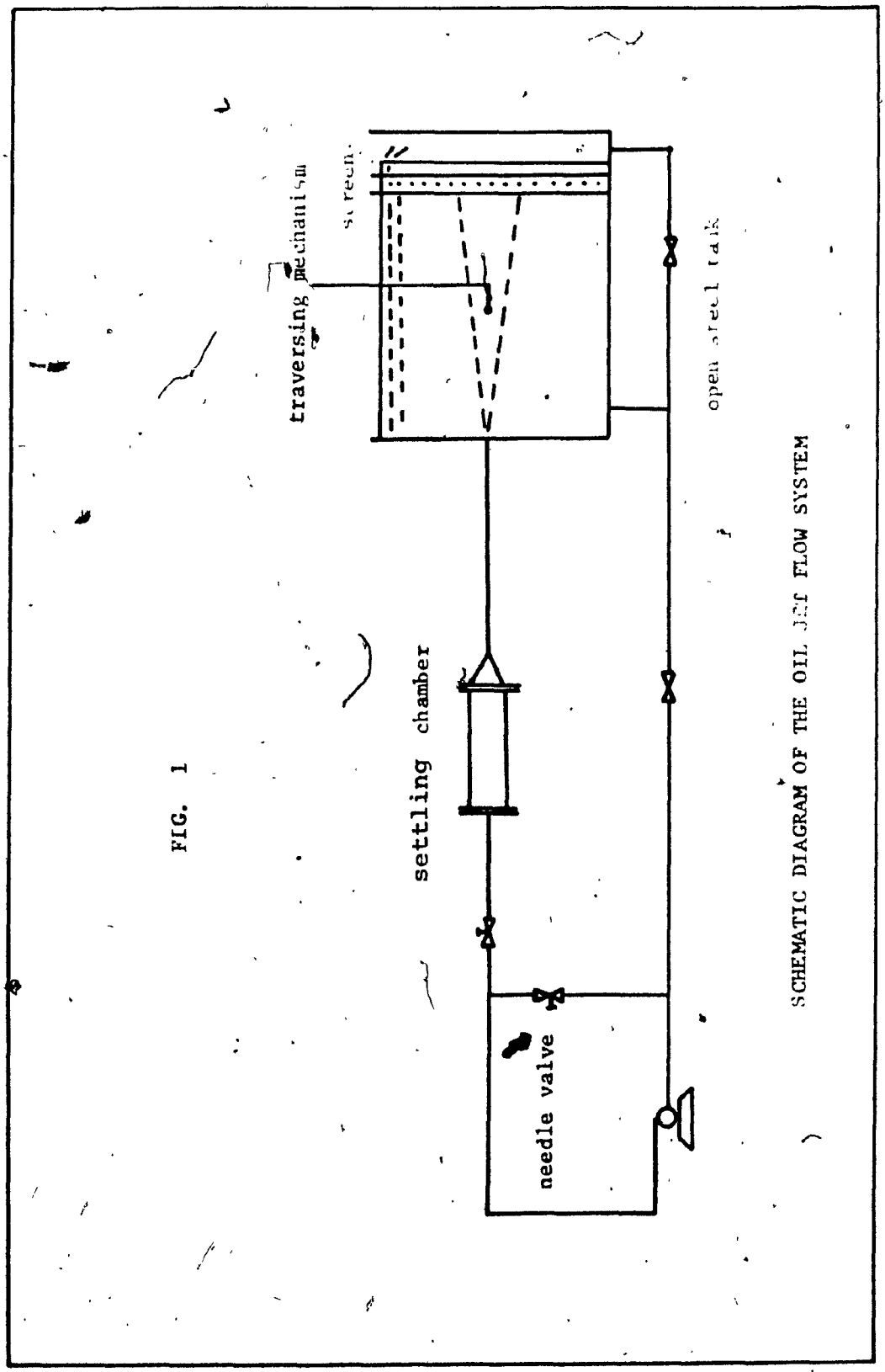

FIG. 1 SCHEMATIC DIAGRAM OF THE OIL JET FLOW SYSTEM

FIG. 2

VELOCITY PROFILE AT THE ORIFICE

OF CALIBRATION

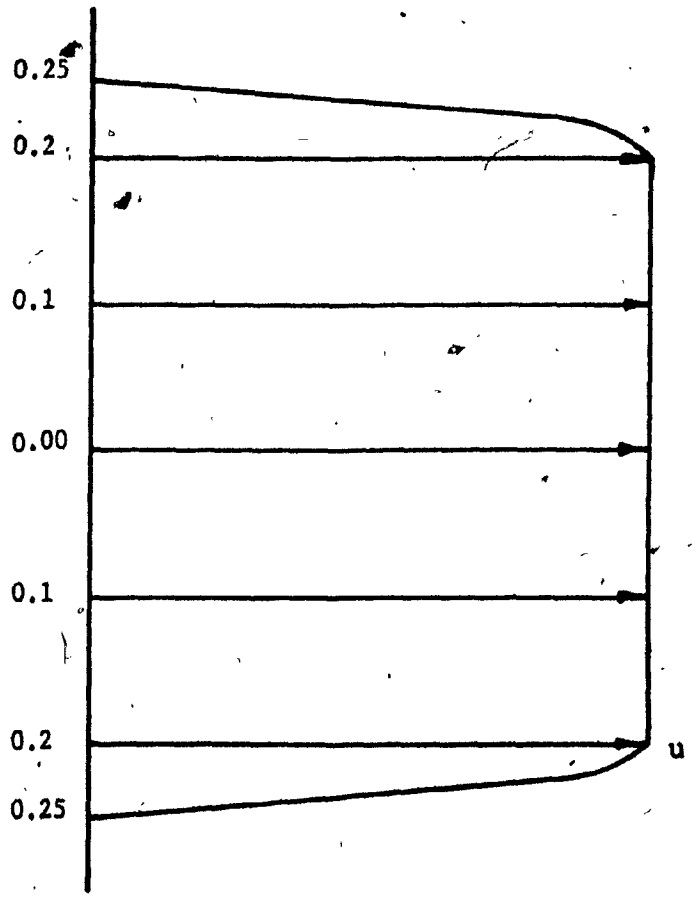

FIG. 3

CALIBRATION OF HOT-FILM PROBE

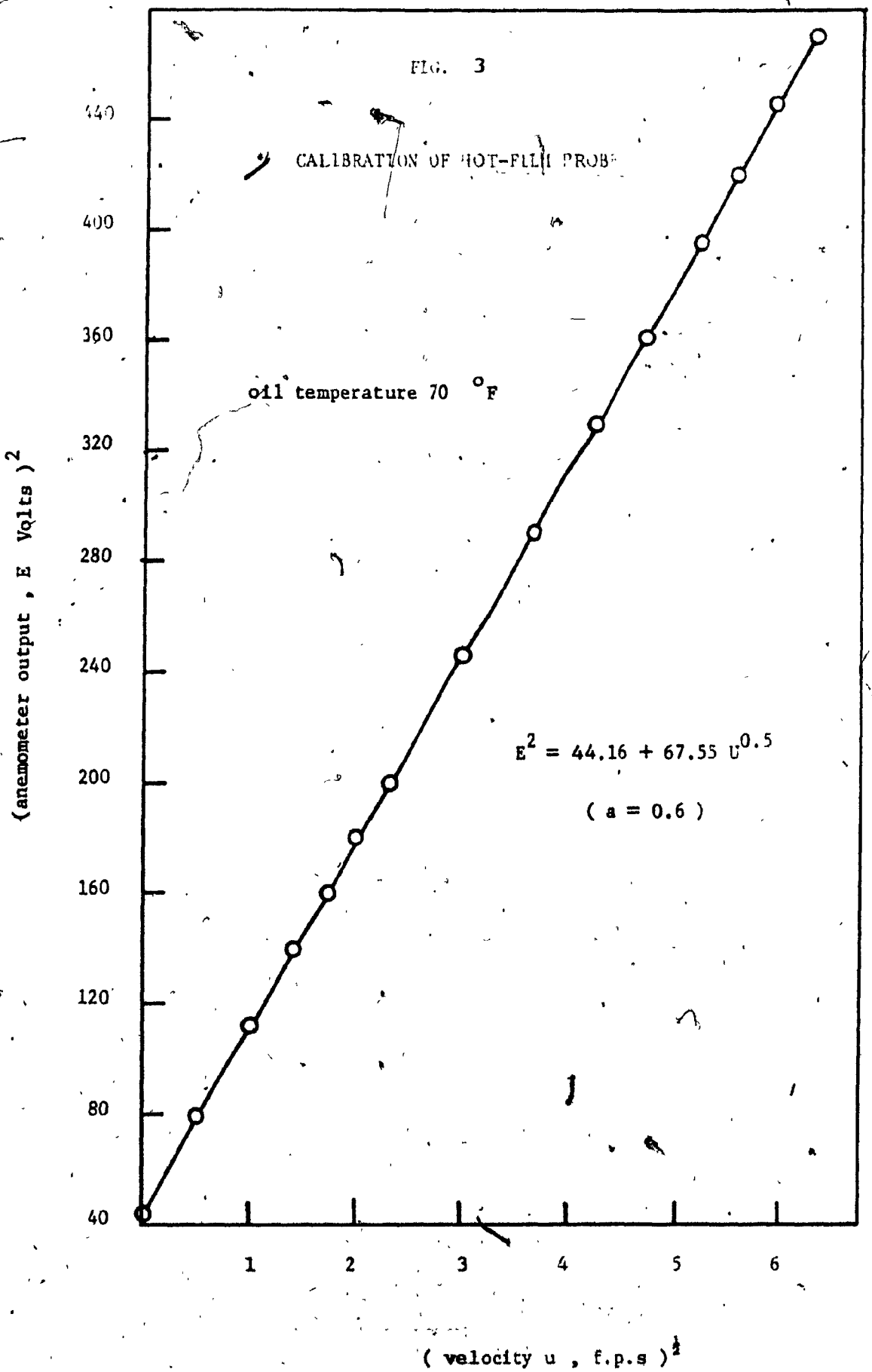

FIG. 4

SAYBOLT UNIVERSAL VISCOSITY CHART

FOR FAXAM 40

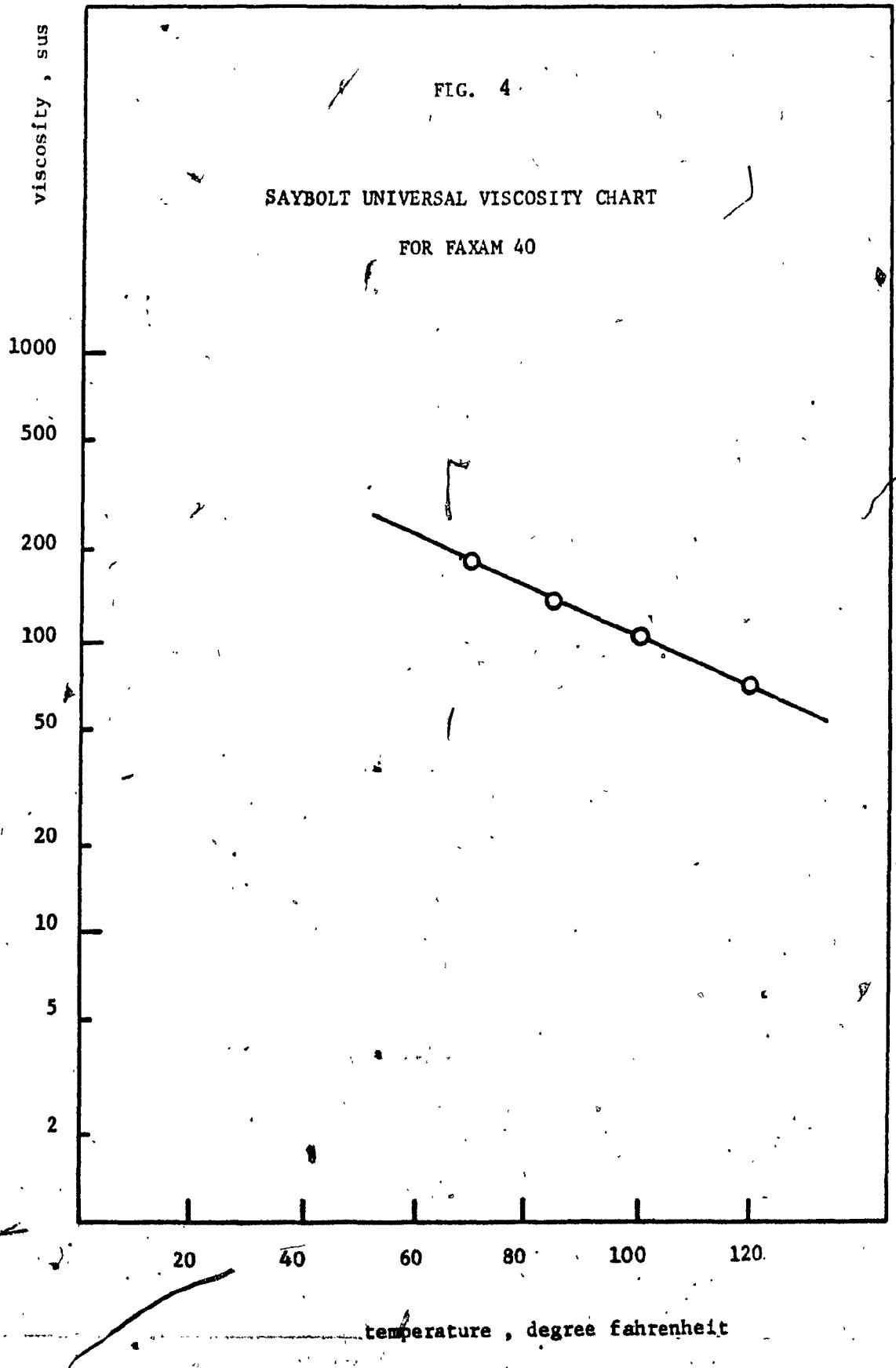

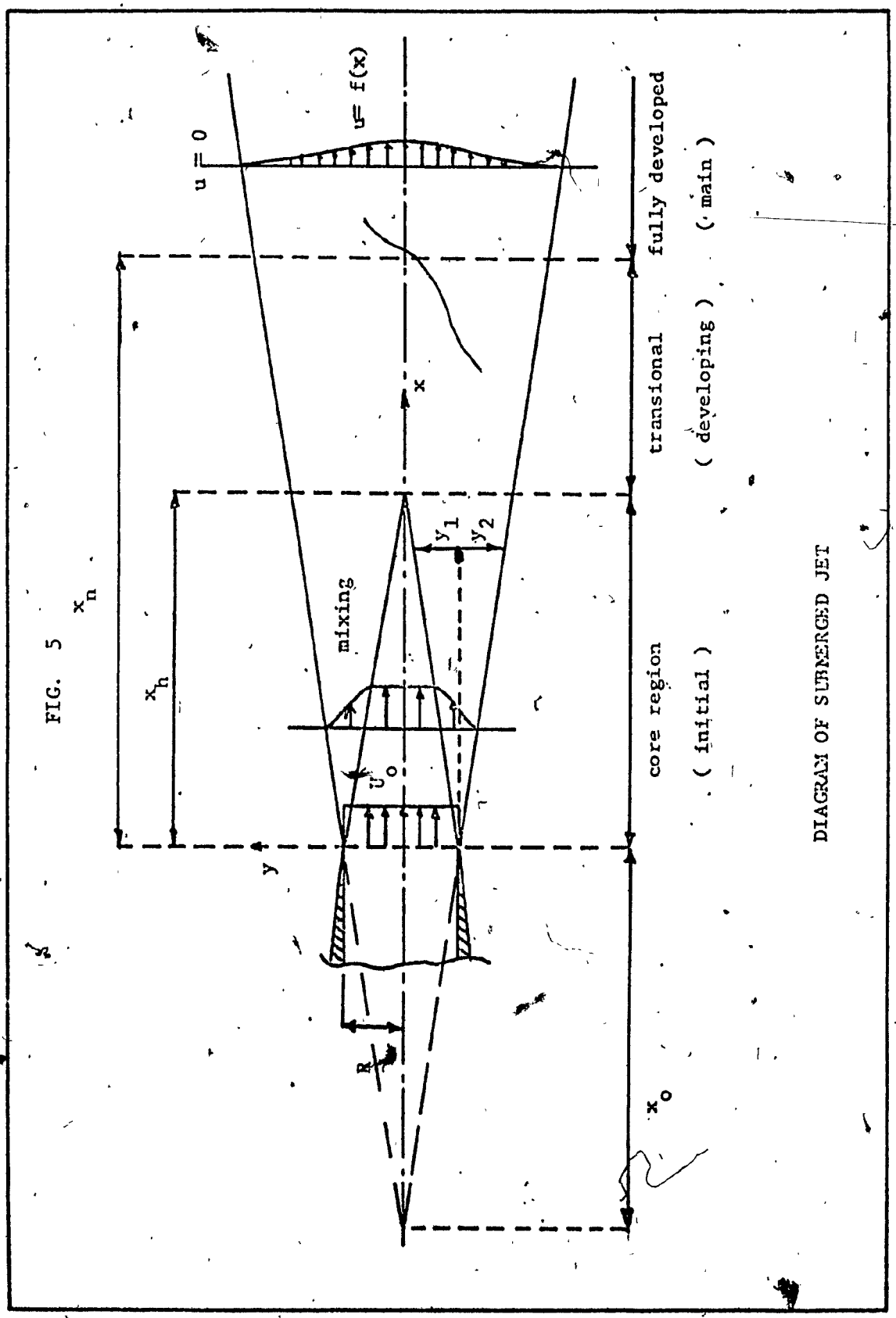

FIG. 5 DIAGRAM OF SUBMERGED JET

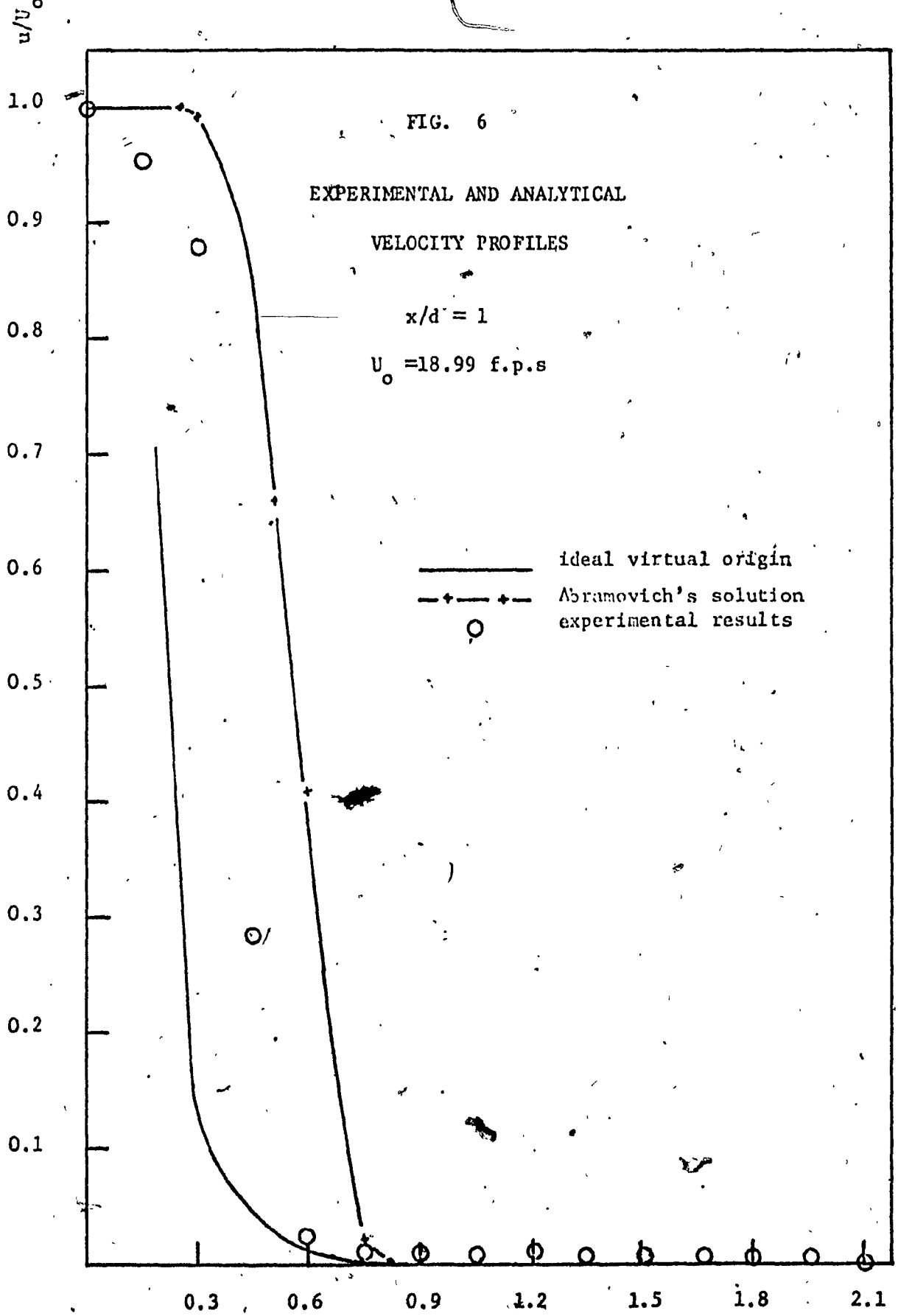

FIG. 6

EXPERIMENTAL AND ANALYTICAL

VELOCITY PROFILES

$x/d = 1$

$U_o = 18.99$ f.p.s

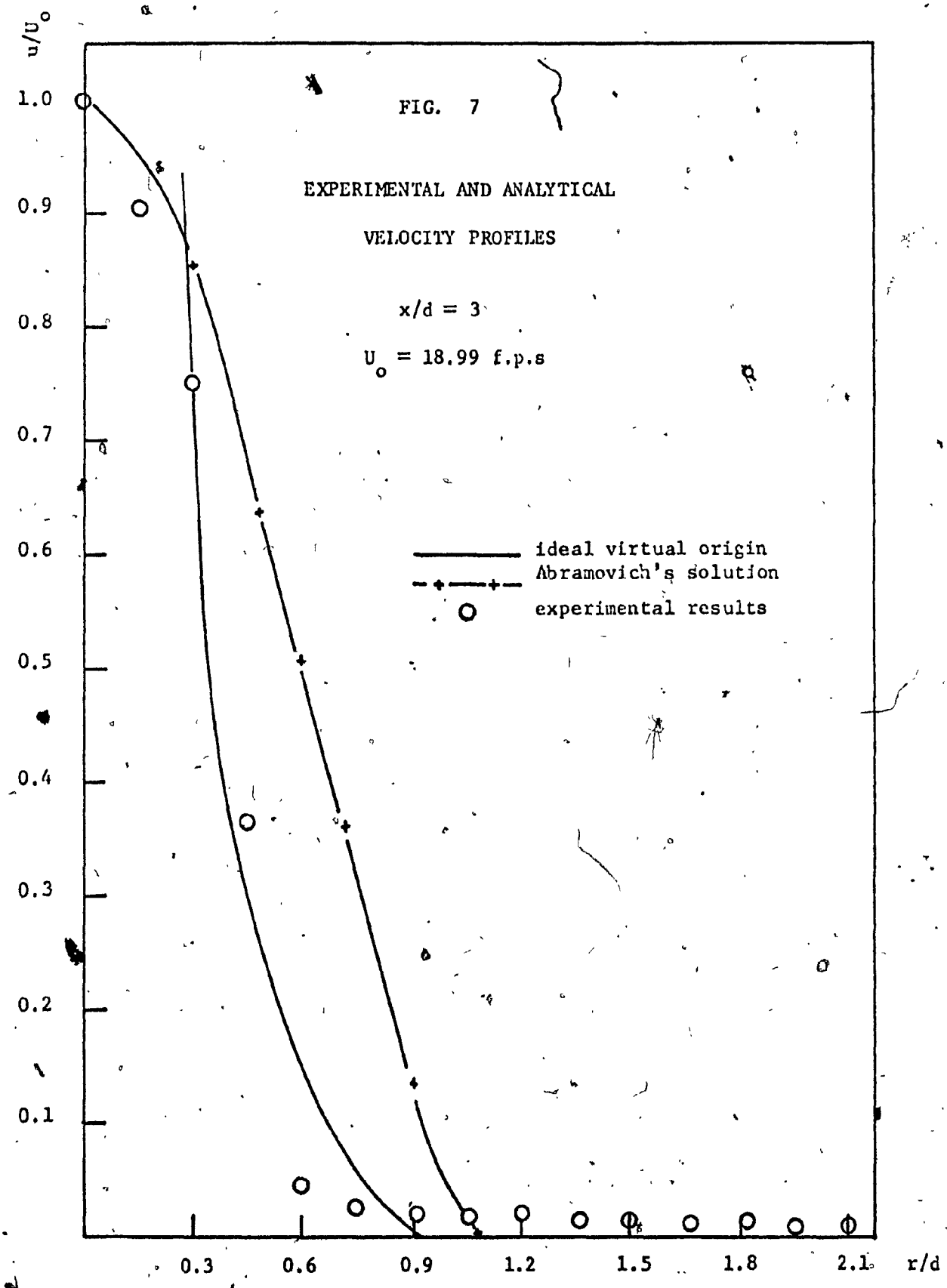

FIG. 7

EXPERIMENTAL AND ANALYTICAL

VELOCITY PROFILES

$x/d = 3$

$U_o = 18.99$ f.p.s

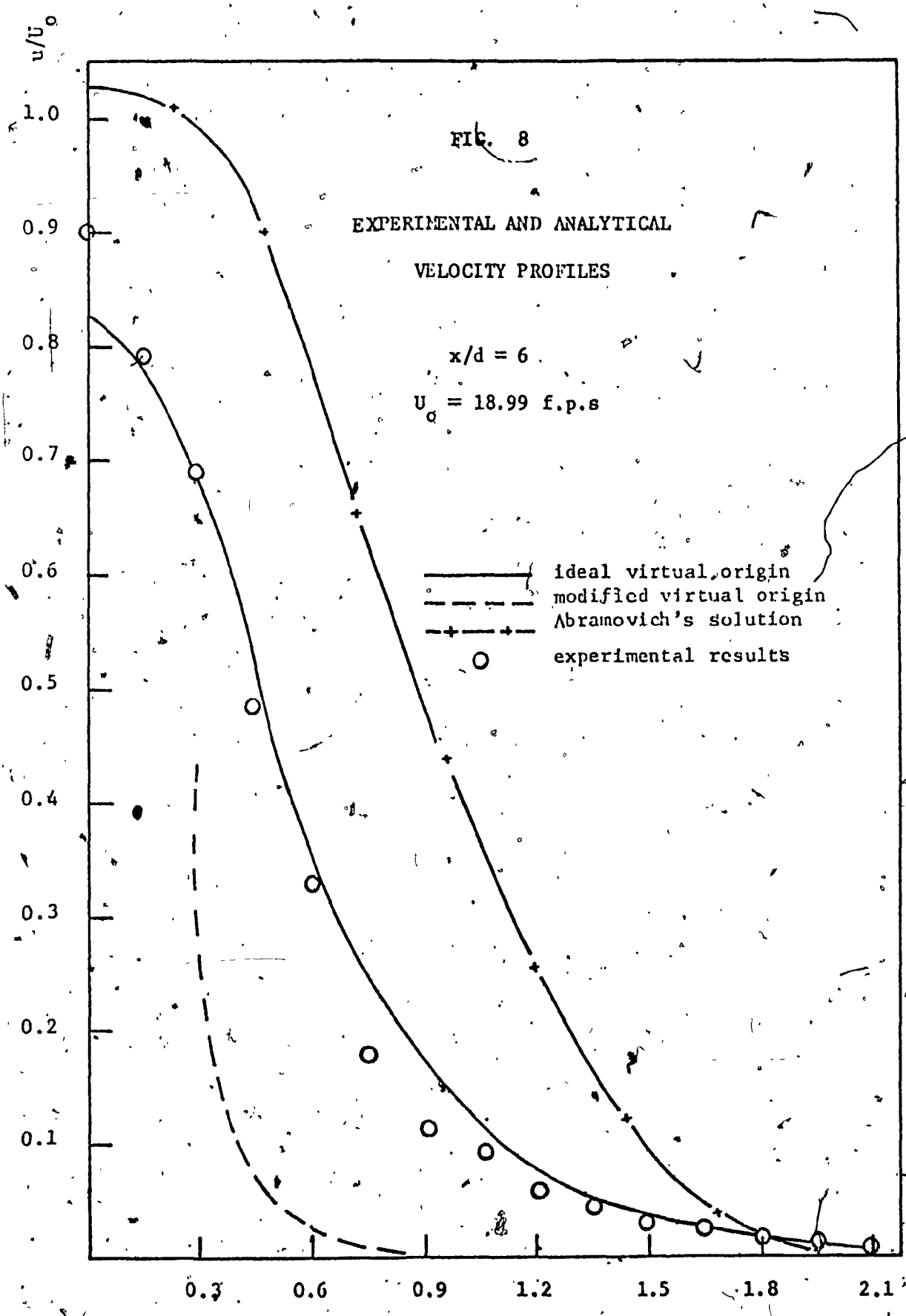

FIG. 8

EXPERIMENTAL AND ANALYTICAL

VELOCITY PROFILES

$x/d = 6$

$U_o = 18.99$ f.p.s

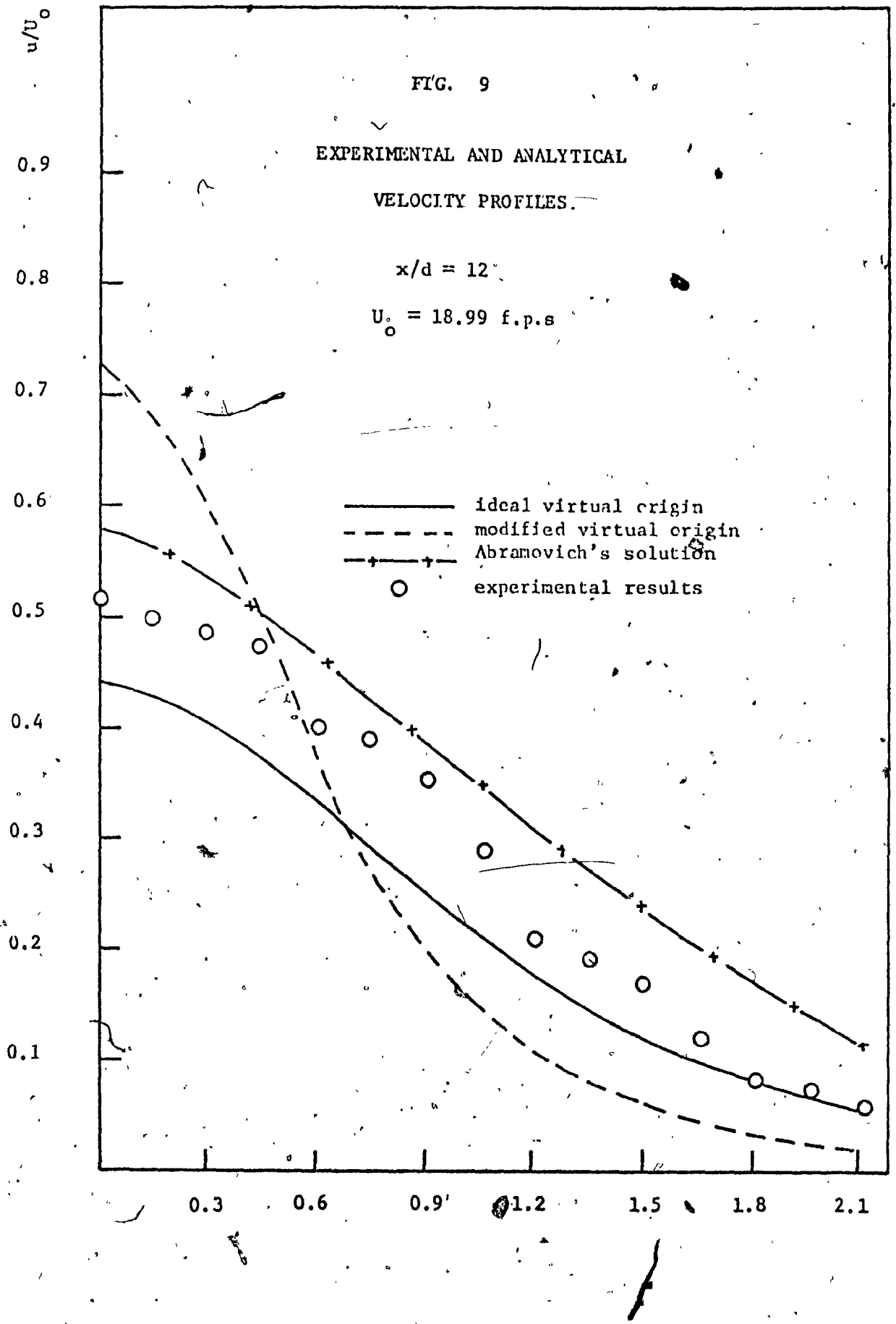

FIG. 9

EXPERIMENTAL AND ANALYTICAL

VELOCITY PROFILES.

x/d = 12

U_o = 18.99 f.p.s

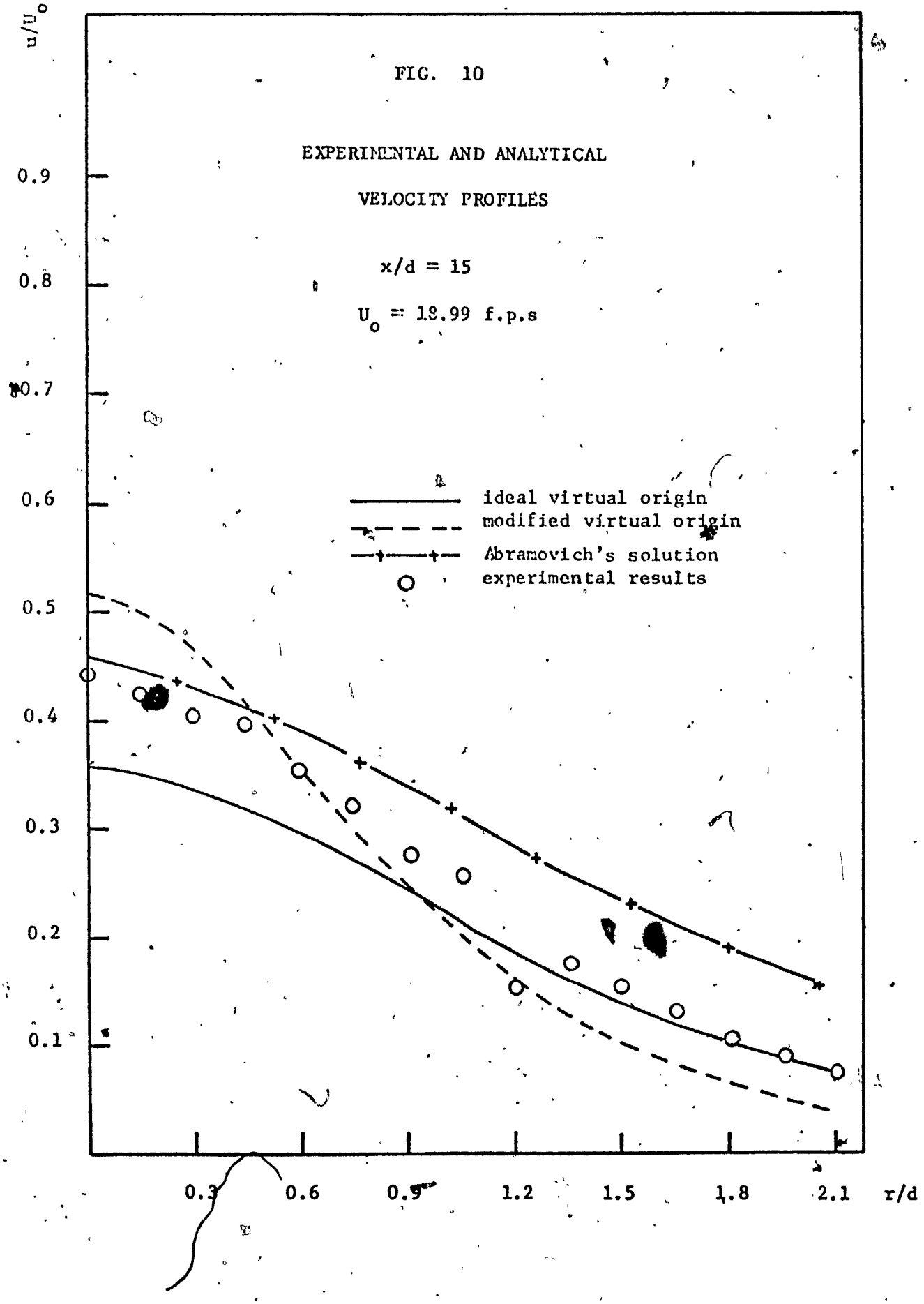

FIG. 10

EXPERIMENTAL AND ANALYTICAL

VELOCITY PROFILES

x/d = 15

U_o = 18.99 f.p.s

FIG. 11

EXPERIMENTAL AND ANALYTICAL

VELOCITY PROFILES

$x/d = 18$

$U_o = 18.99$ f.p.s

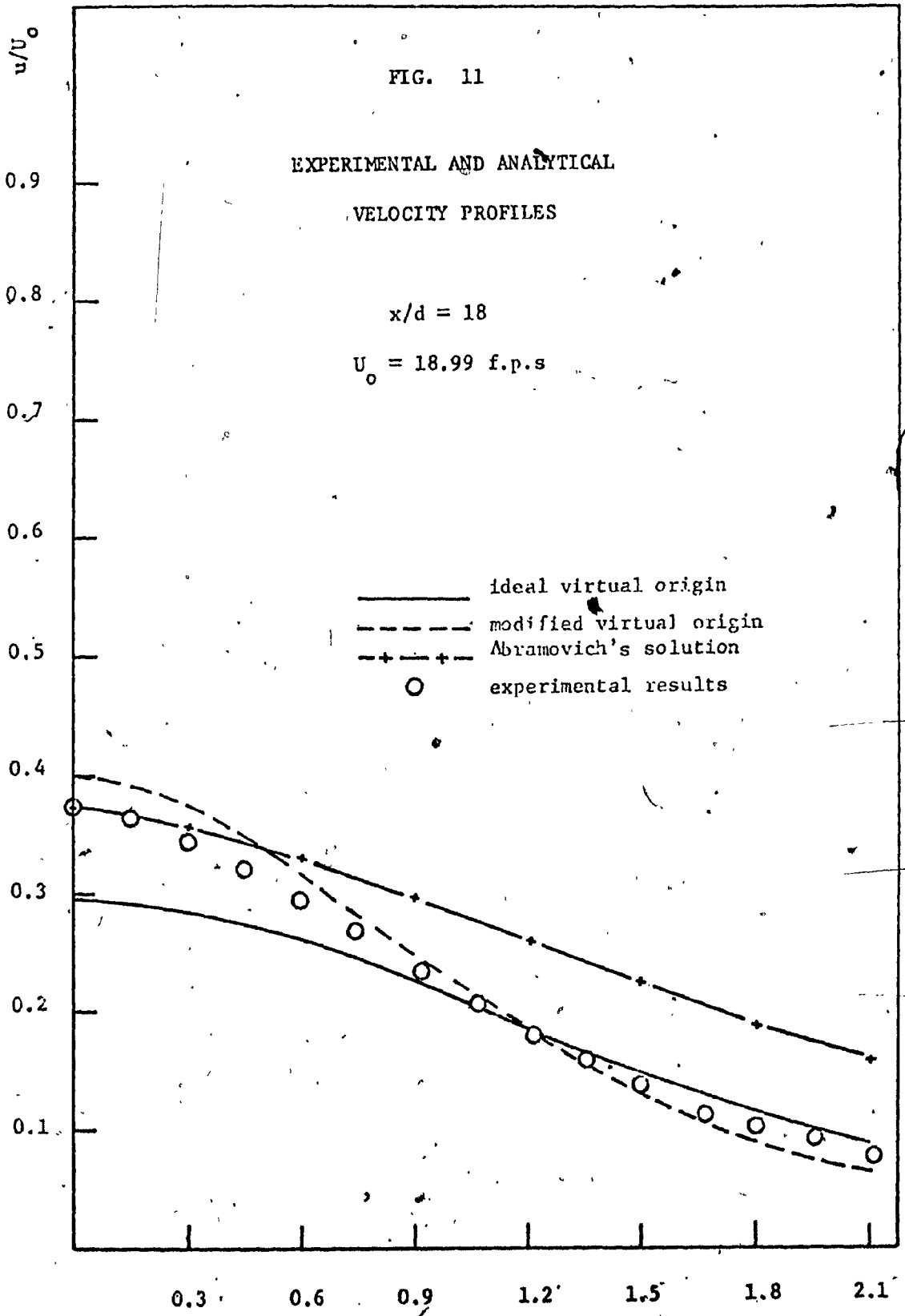

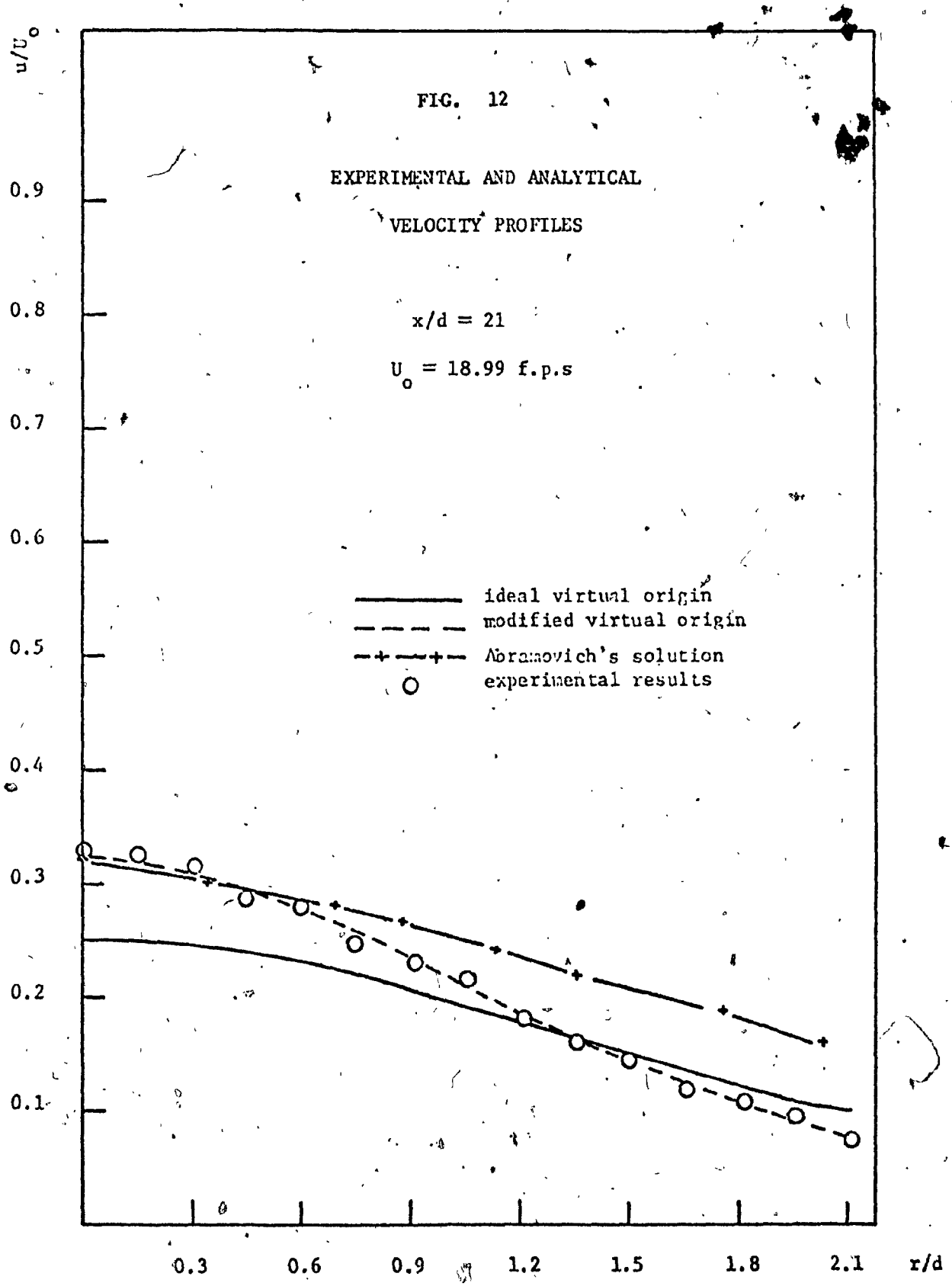

FIG. 12

EXPERIMENTAL AND ANALYTICAL

VELOCITY PROFILES

$x/d = 21$

$U_o = 18.99$ f.p.s

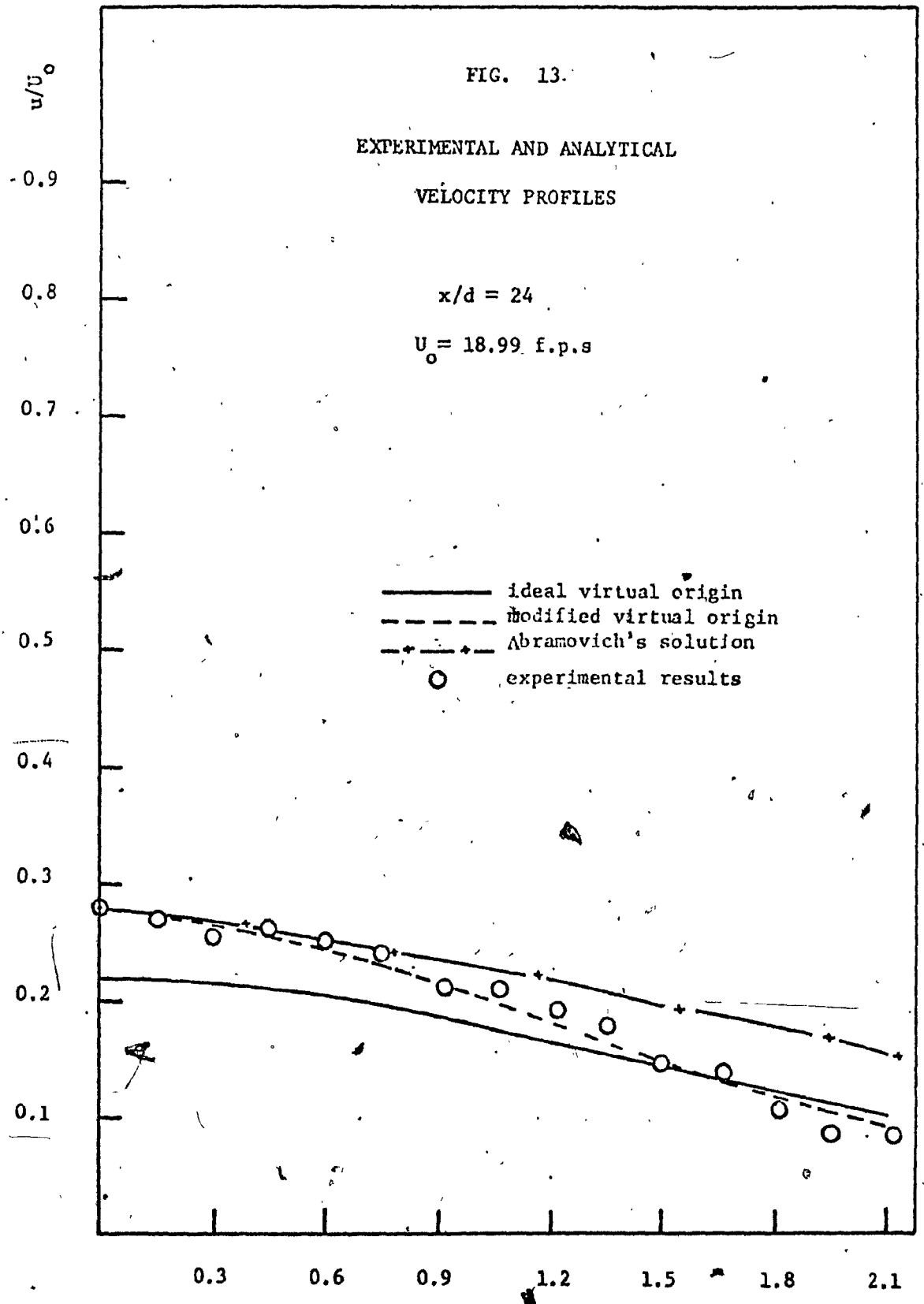

FIG. 13.

EXPERIMENTAL AND ANALYTICAL

VELOCITY PROFILES

$x/d = 24$

$U_o = 18.99$ f.p.s

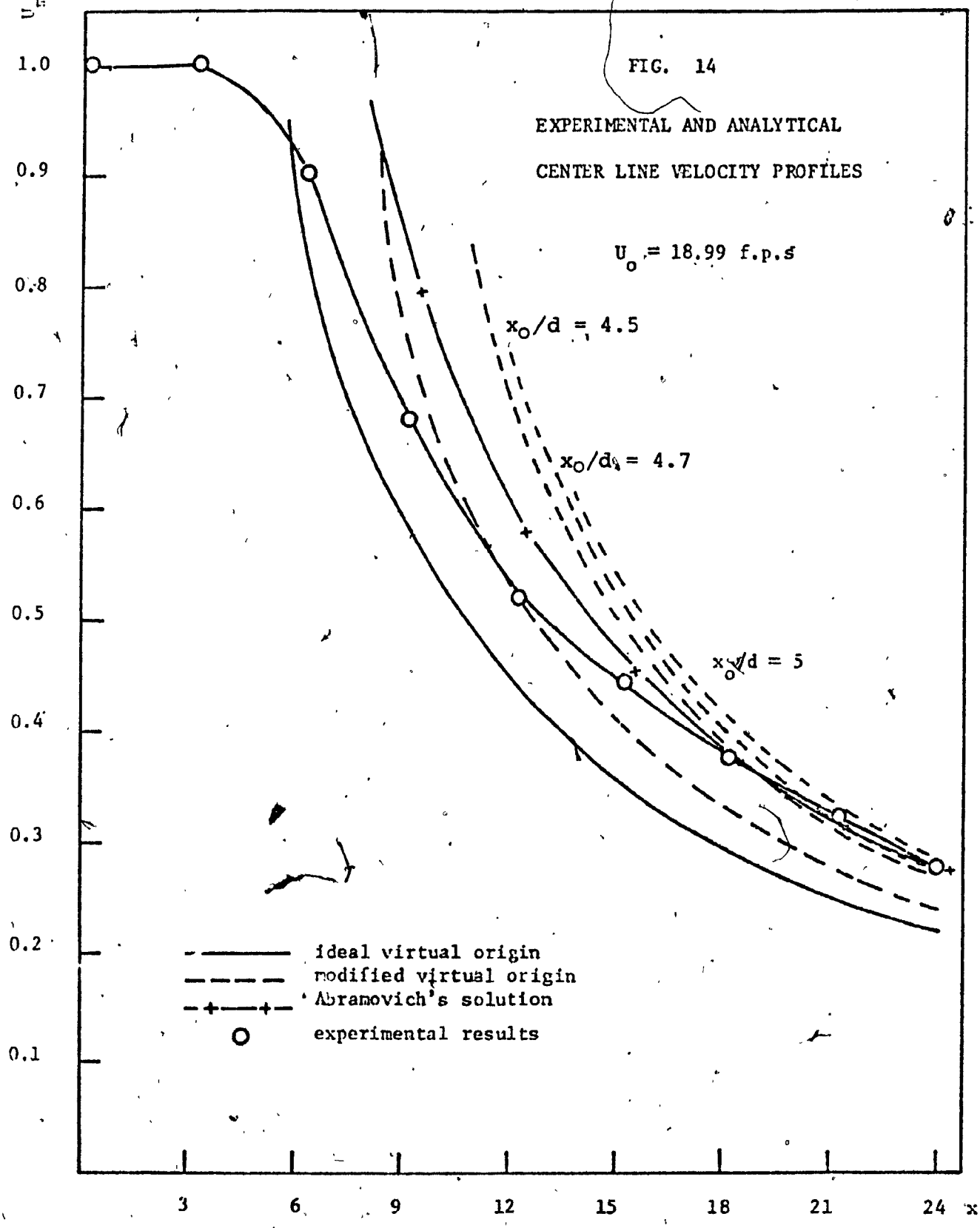

FIG. 14

EXPERIMENTAL AND ANALYTICAL

CENTER LINE VELOCITY PROFILES

$U_o = 18.99$ f.p.s

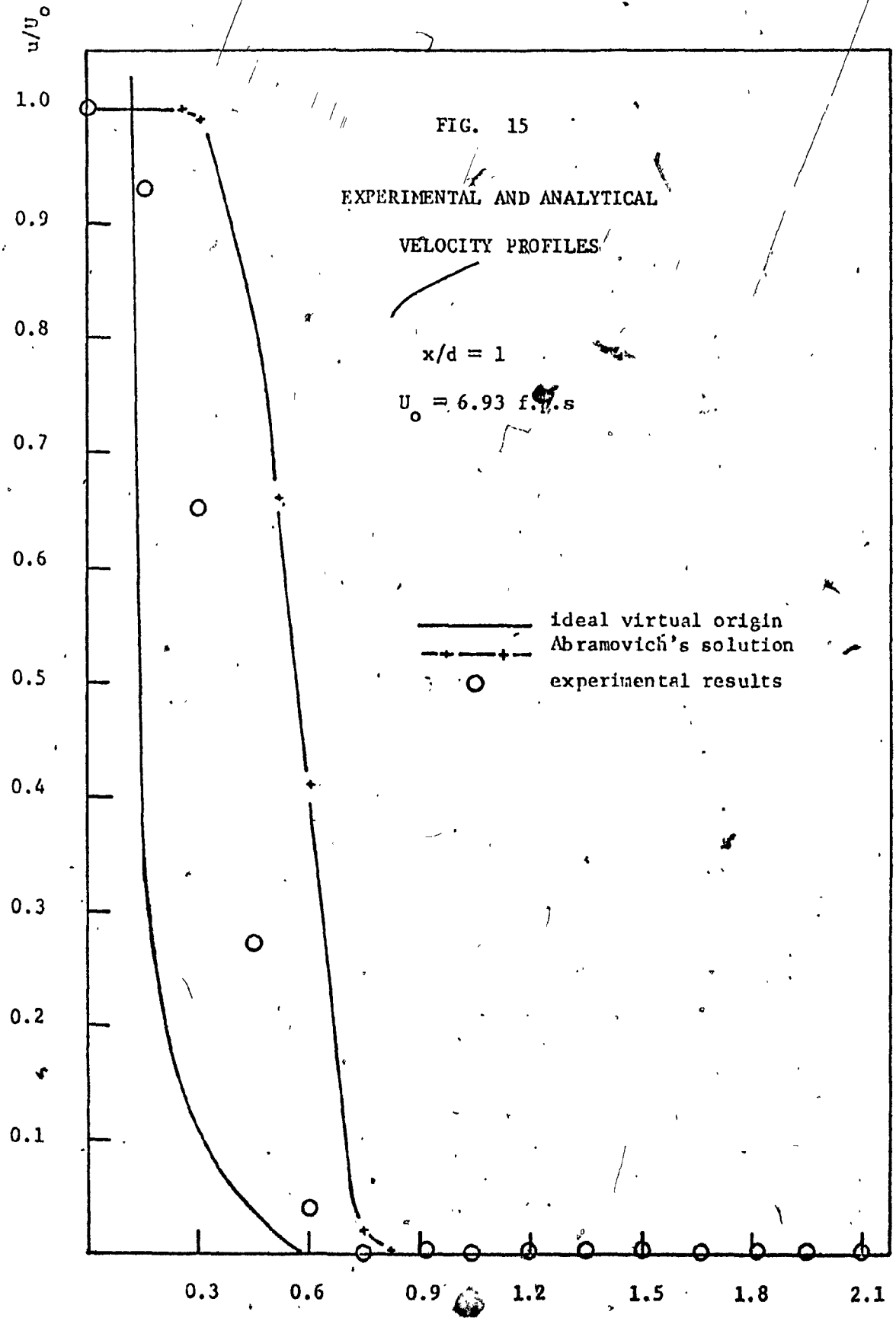

FIG. 15

EXPERIMENTAL AND ANALYTICAL VELOCITY PROFILES

$x/d = 1$

$U_o = 6.93$ f.p.s

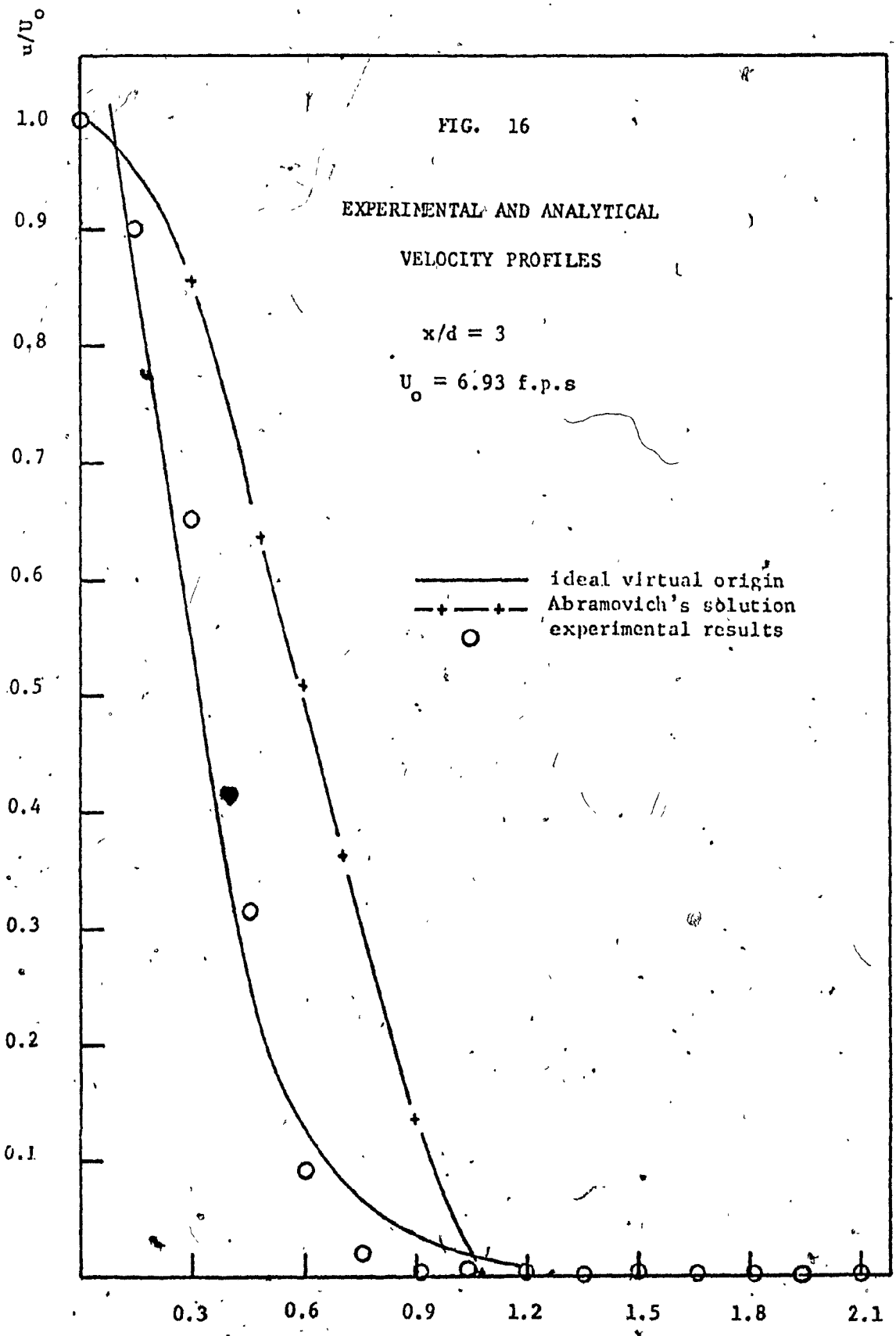

FIG. 16

EXPERIMENTAL AND ANALYTICAL

VELOCITY PROFILES

$x/d = 3$

$U_o = 6.93$ f.p.s

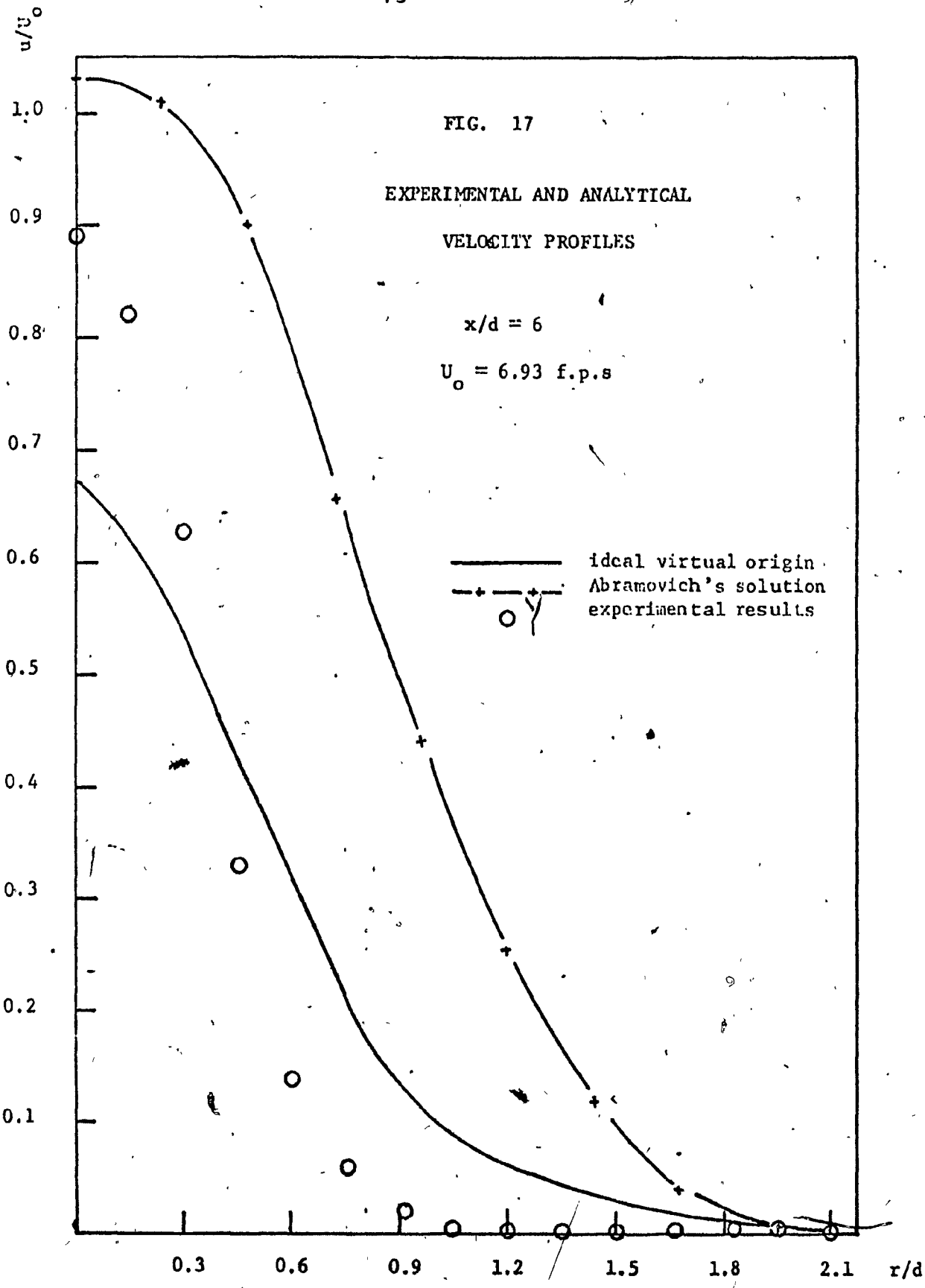

FIG. 17

EXPERIMENTAL AND ANALYTICAL

VELOCITY PROFILES

$x/d = 6$

$U_o = 6.93$ f.p.s

FIG. 18

EXPERIMENTAL AND ANALYTICAL

VELOCITY PROFILES

$x/d = 12$

$U_o = 6.93$ f.p.s

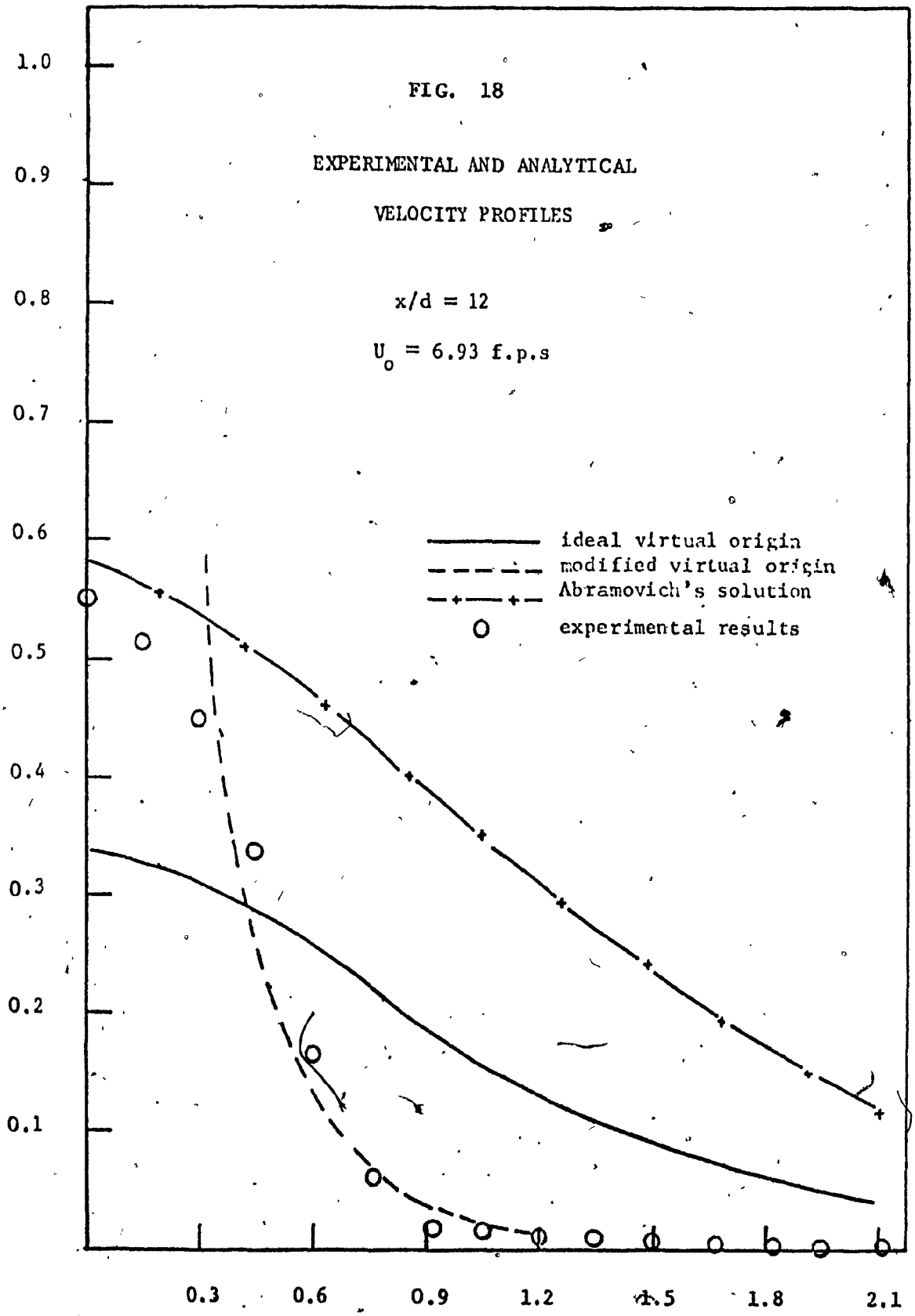

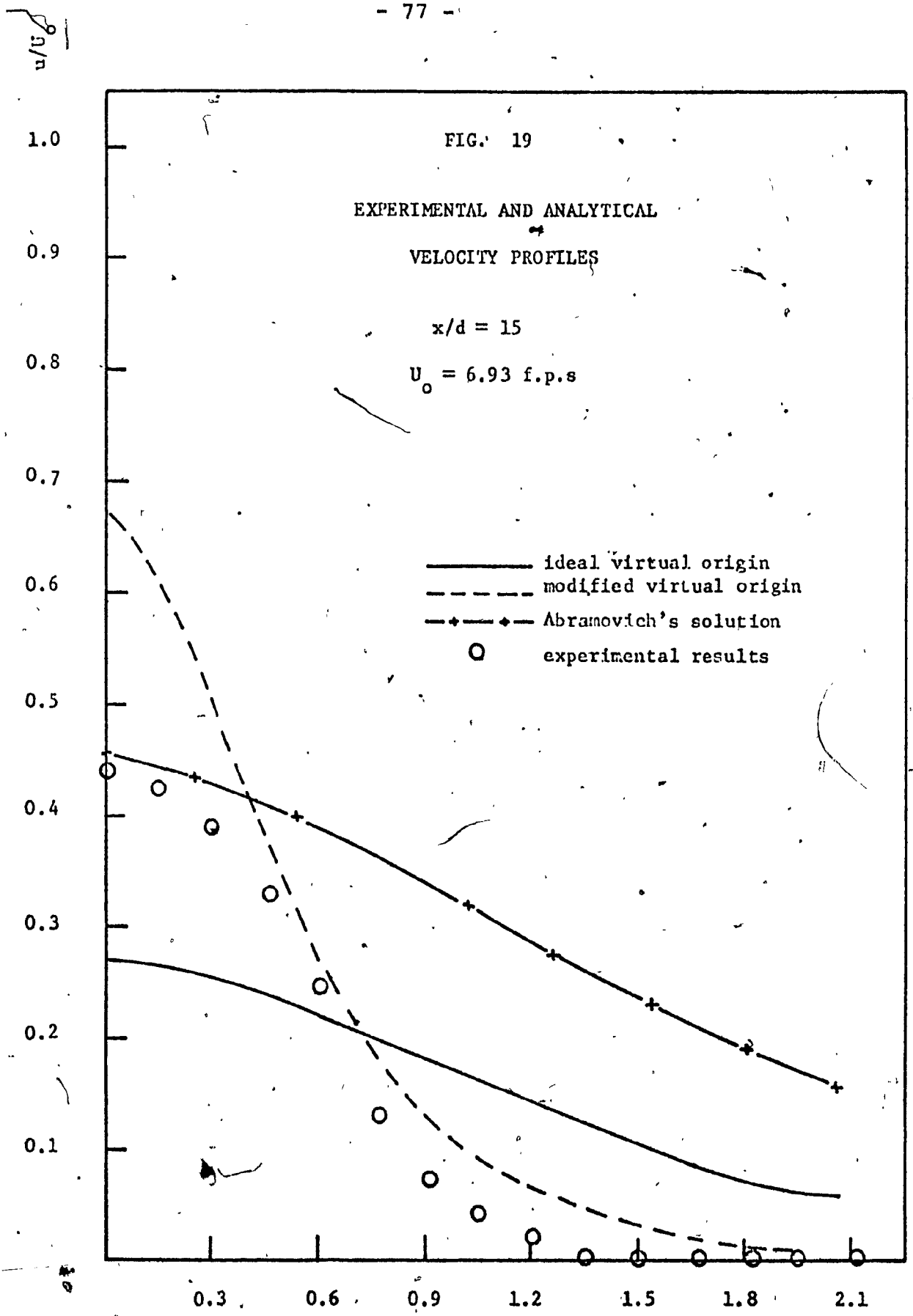

FIG. 19

EXPERIMENTAL AND ANALYTICAL

VELOCITY PROFILES

x/d = 15

U_o = 6.93 f.p.s

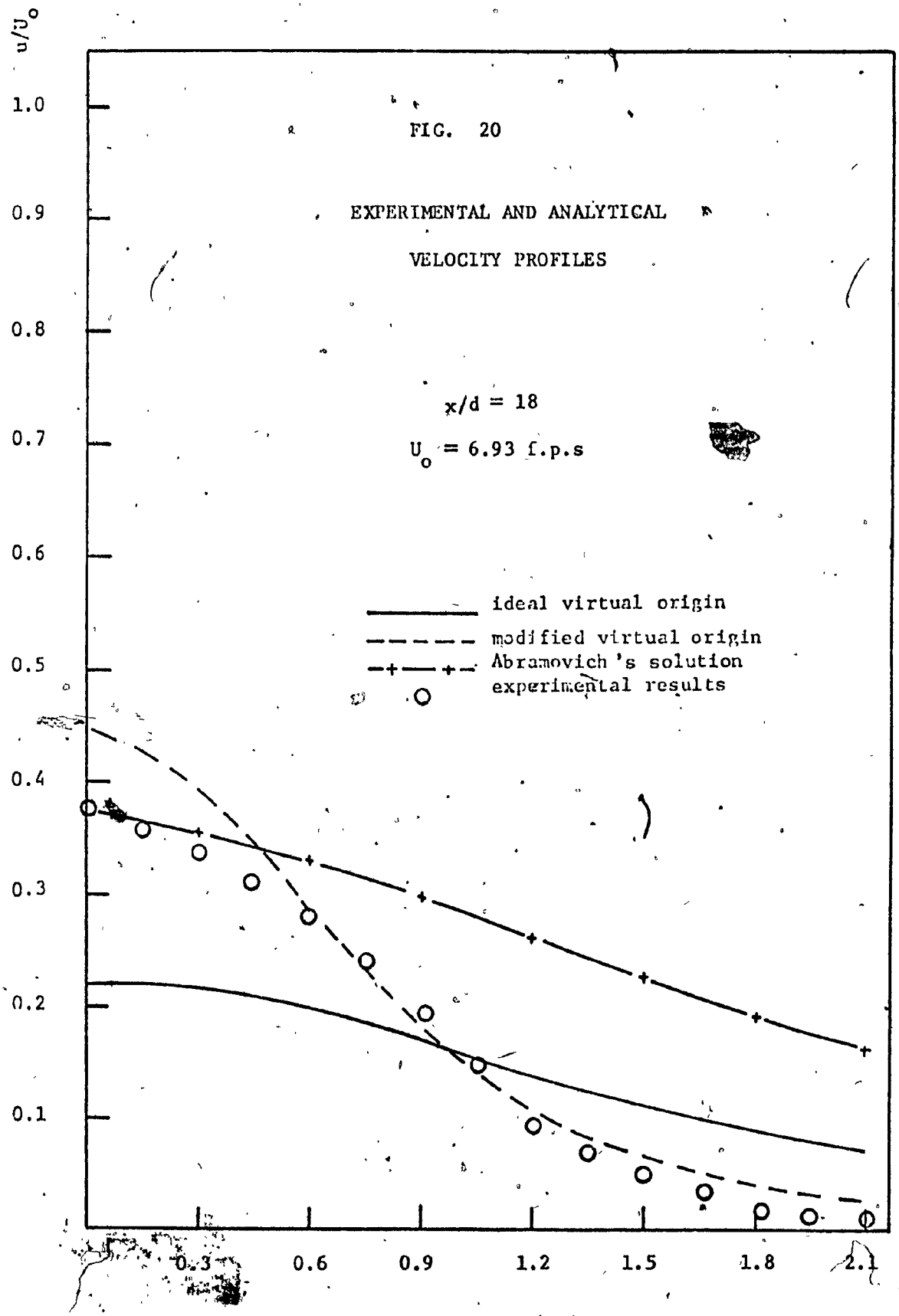

FIG. 20

EXPERIMENTAL AND ANALYTICAL

VELOCITY PROFILES

$x/d = 18$

$U_o = 6.93$ f.p.s

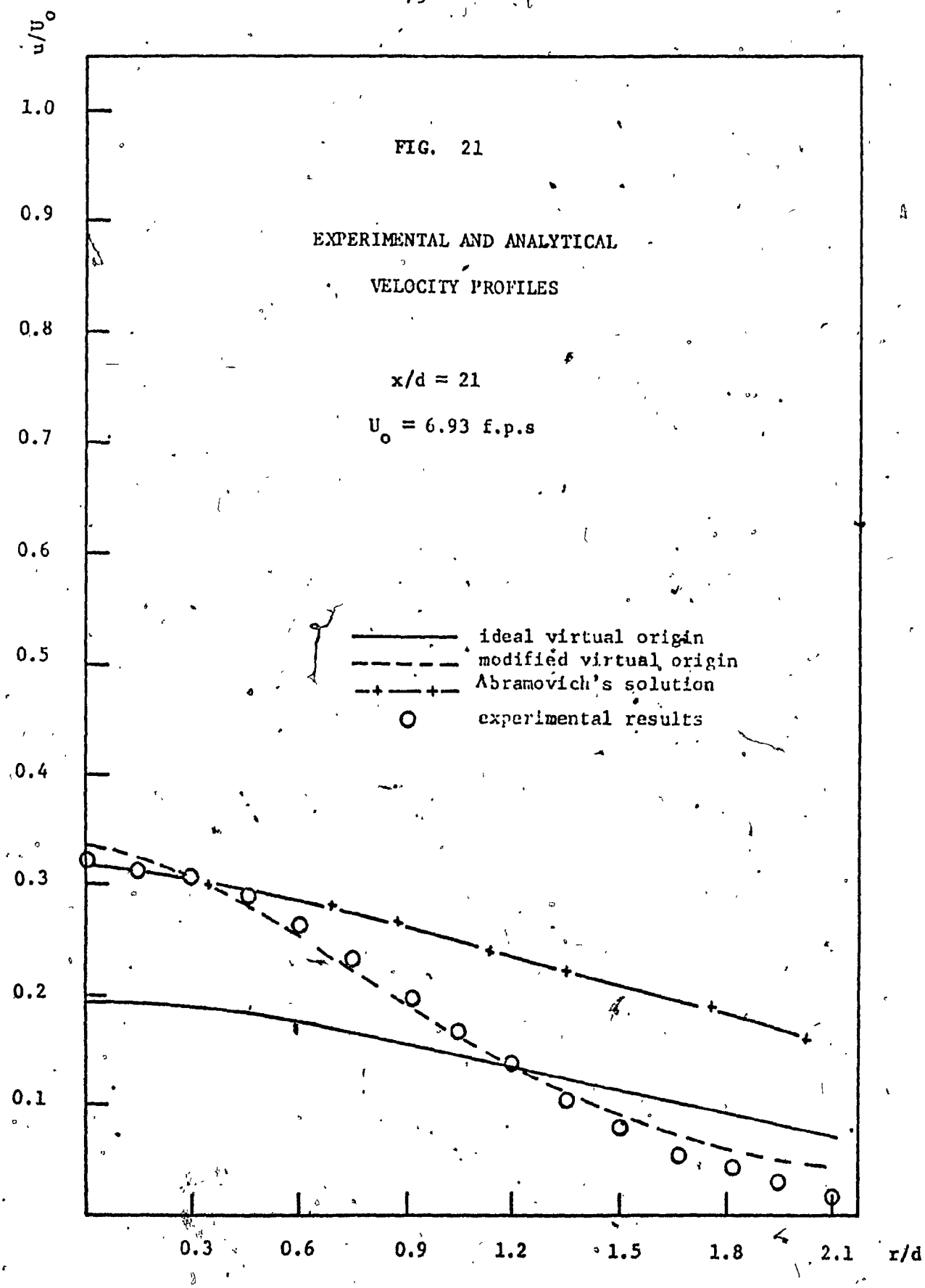

FIG. 21

EXPERIMENTAL AND ANALYTICAL VELOCITY PROFILES

$x/d = 21$

$U_o = 6.93$ f.p.s

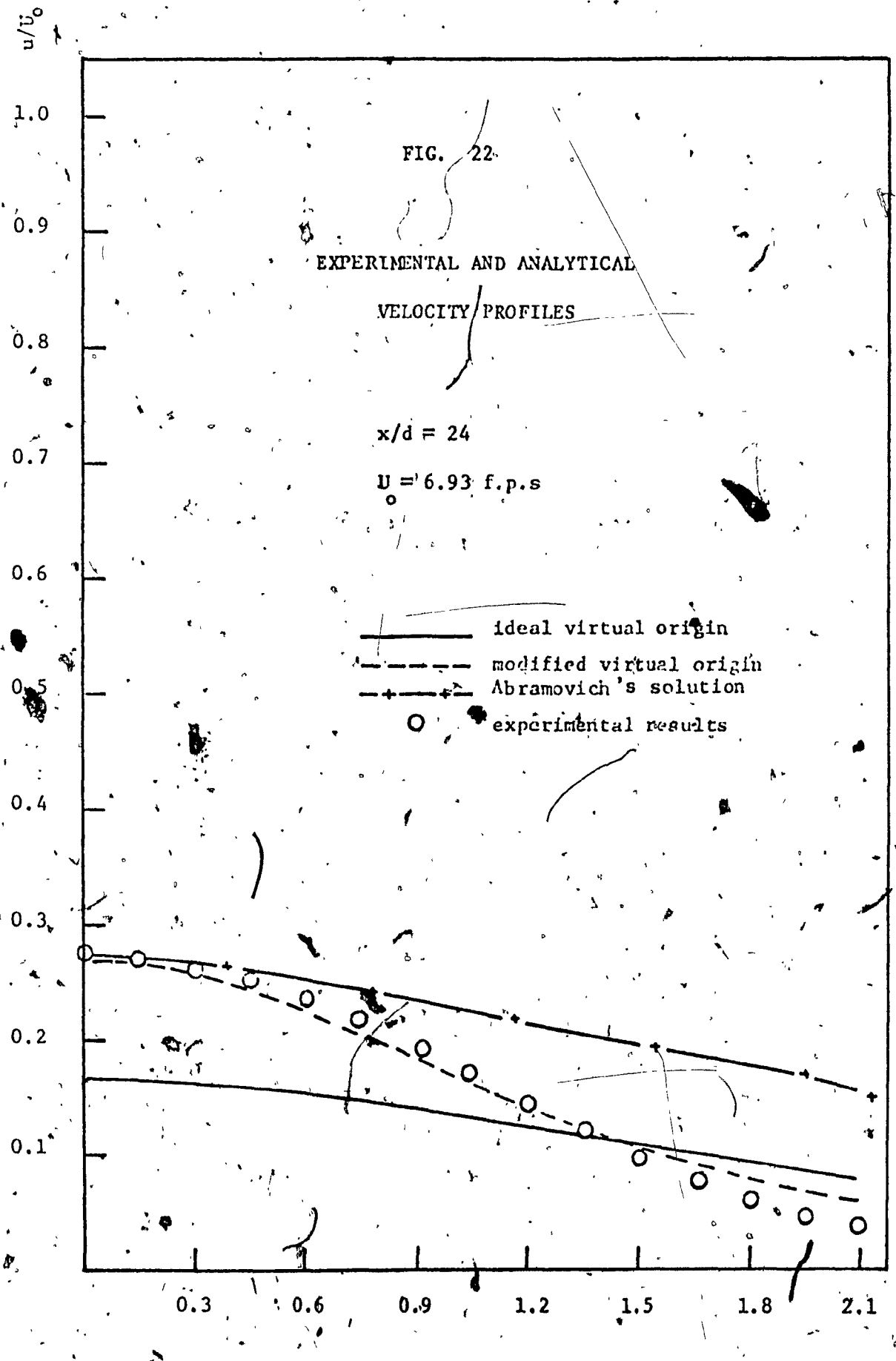

FIG. 22

EXPERIMENTAL AND ANALYTICAL VELOCITY PROFILES

x/d = 24

U_o = 6.93 f.p.s

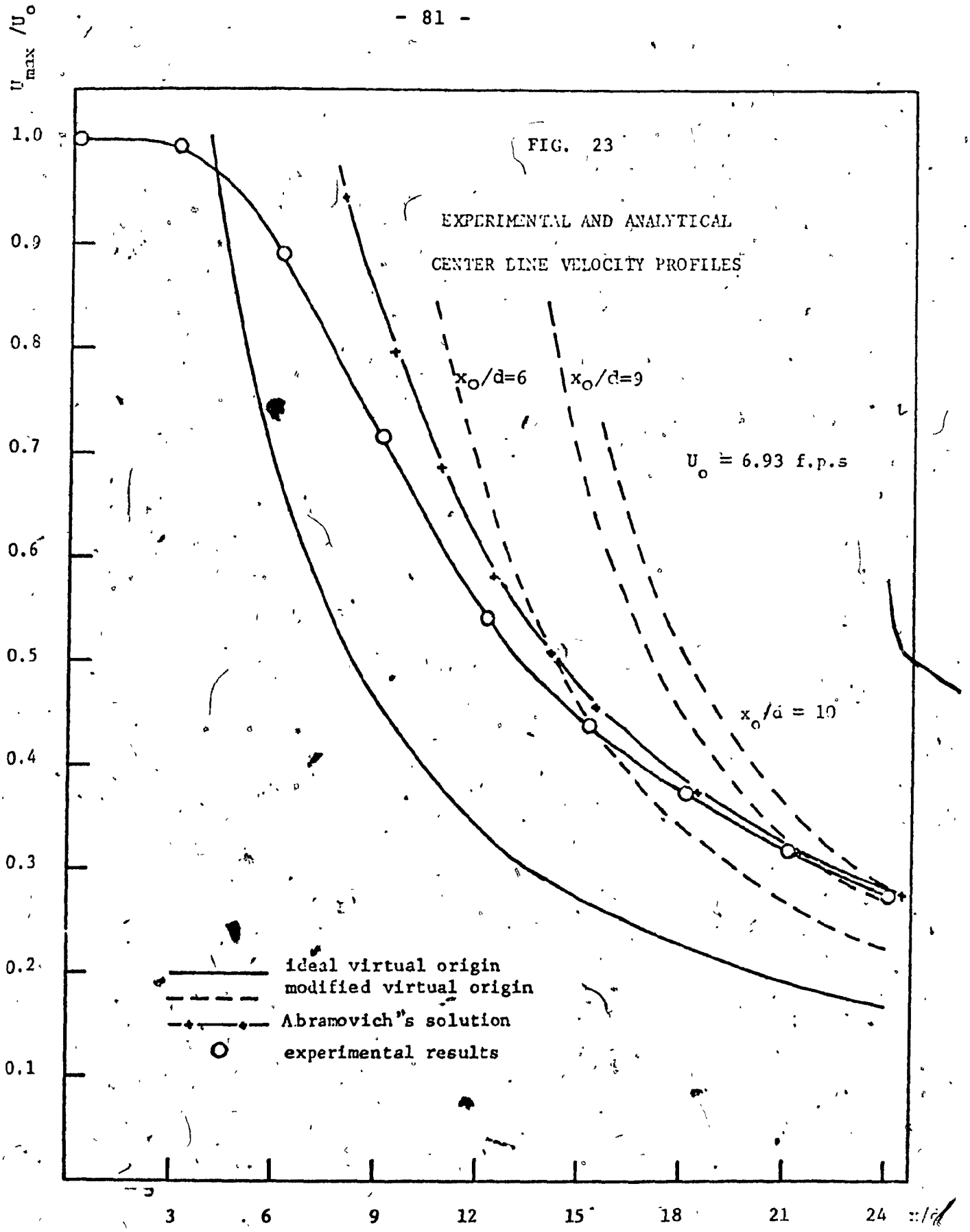

FIG. 23

EXPERIMENTAL AND ANALYTICAL

CENTER LINE VELOCITY PROFILES

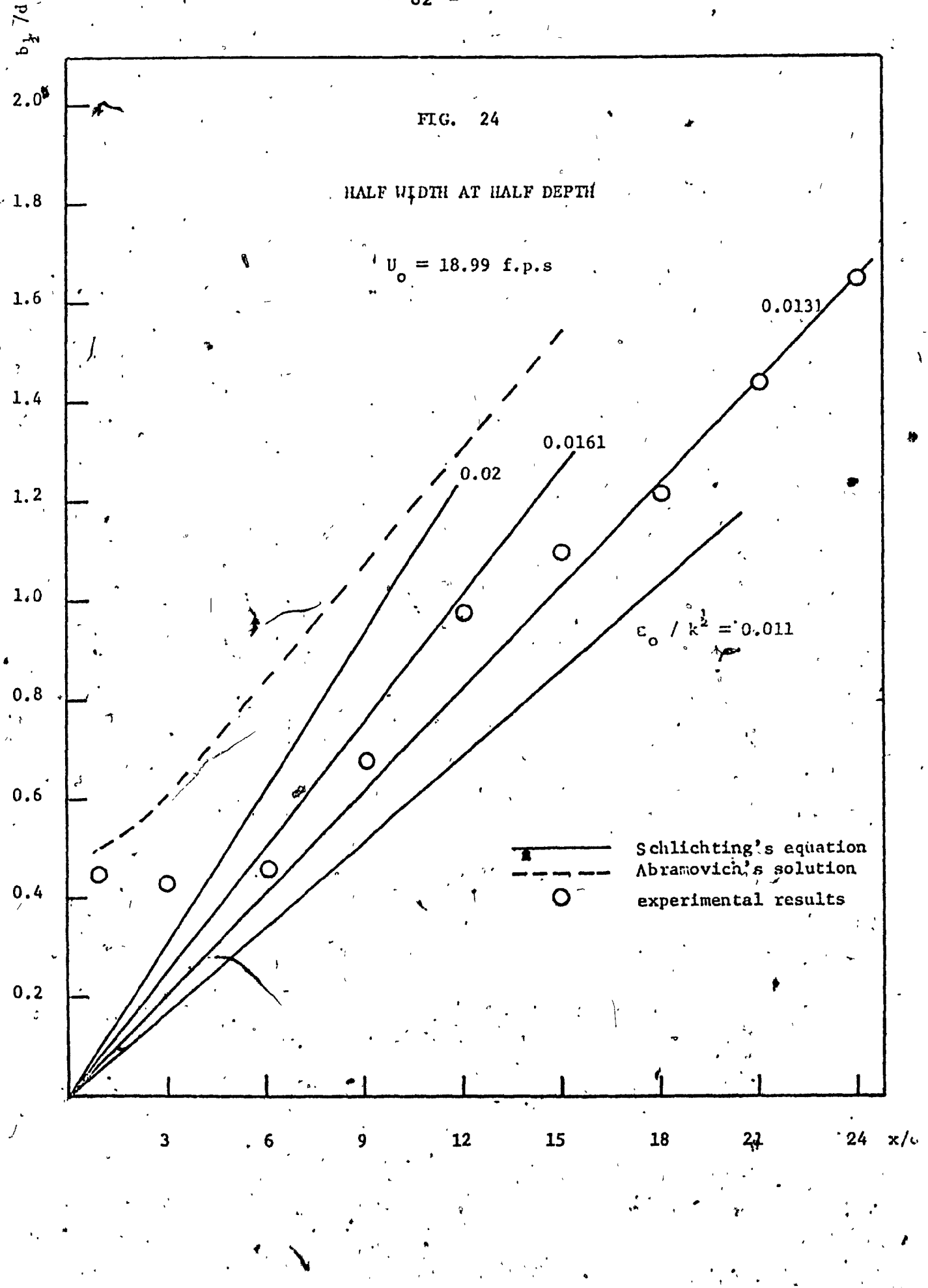

FIG. 24

HALF WIDTH AT HALF DEPTH

U_o = 18.99 f.p.s

FIG. 25

HALF WIDTH AT HALF DEPTH

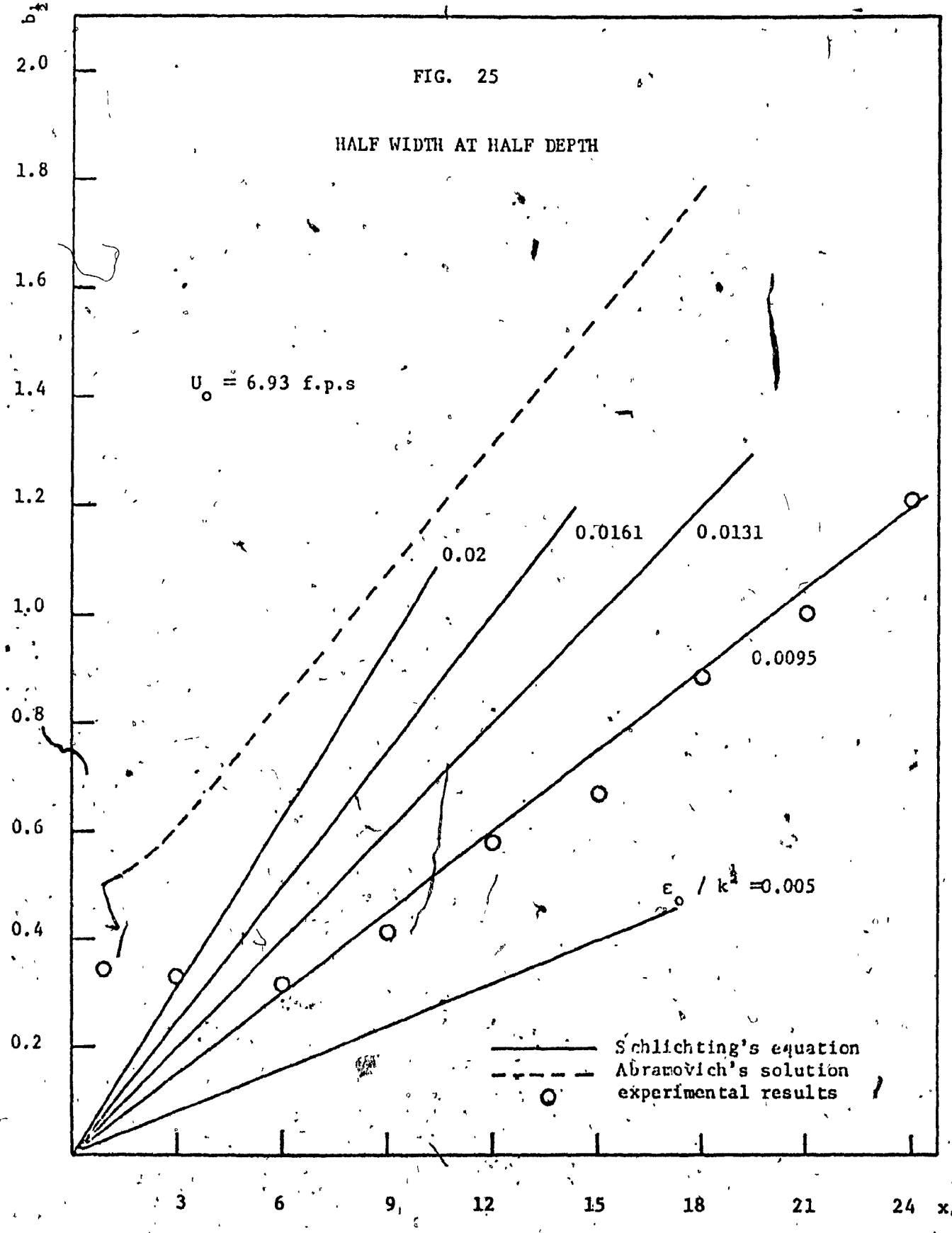

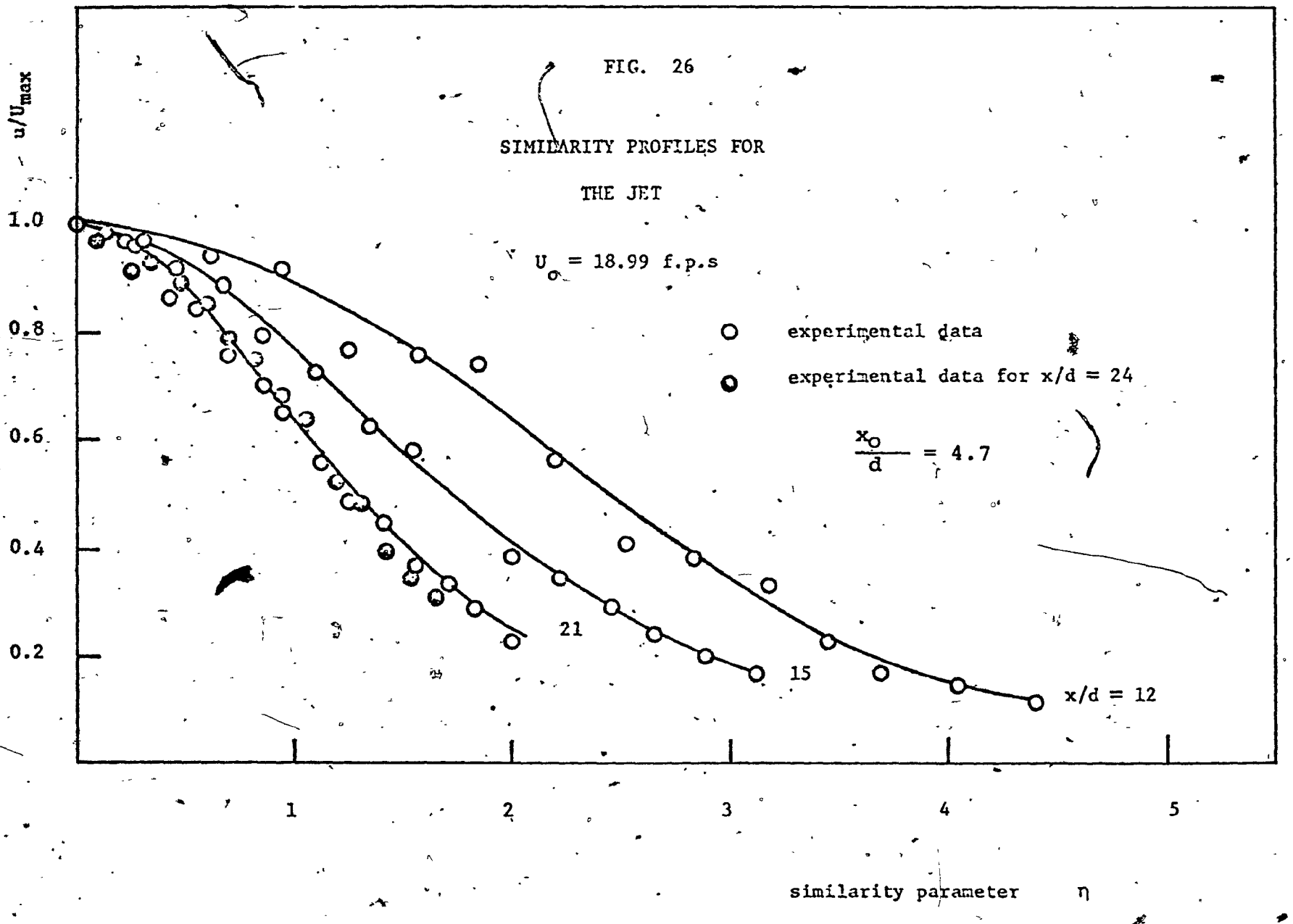
FIG. 26
SIMILARITY PROFILES FOR
THE JET
U_o = 18.99 f.p.s
experimental data
experimental data for x/d = 24
$\frac{x_o}{d}$ = 4.7
u/U_{max}
1.0
0.8
0.6
0.4
0.2
21
15
x/d = 12
1
2
3
4
5
similarity parameter η

FIG. 27

SIMILARITY PROFILES FOR THE JET

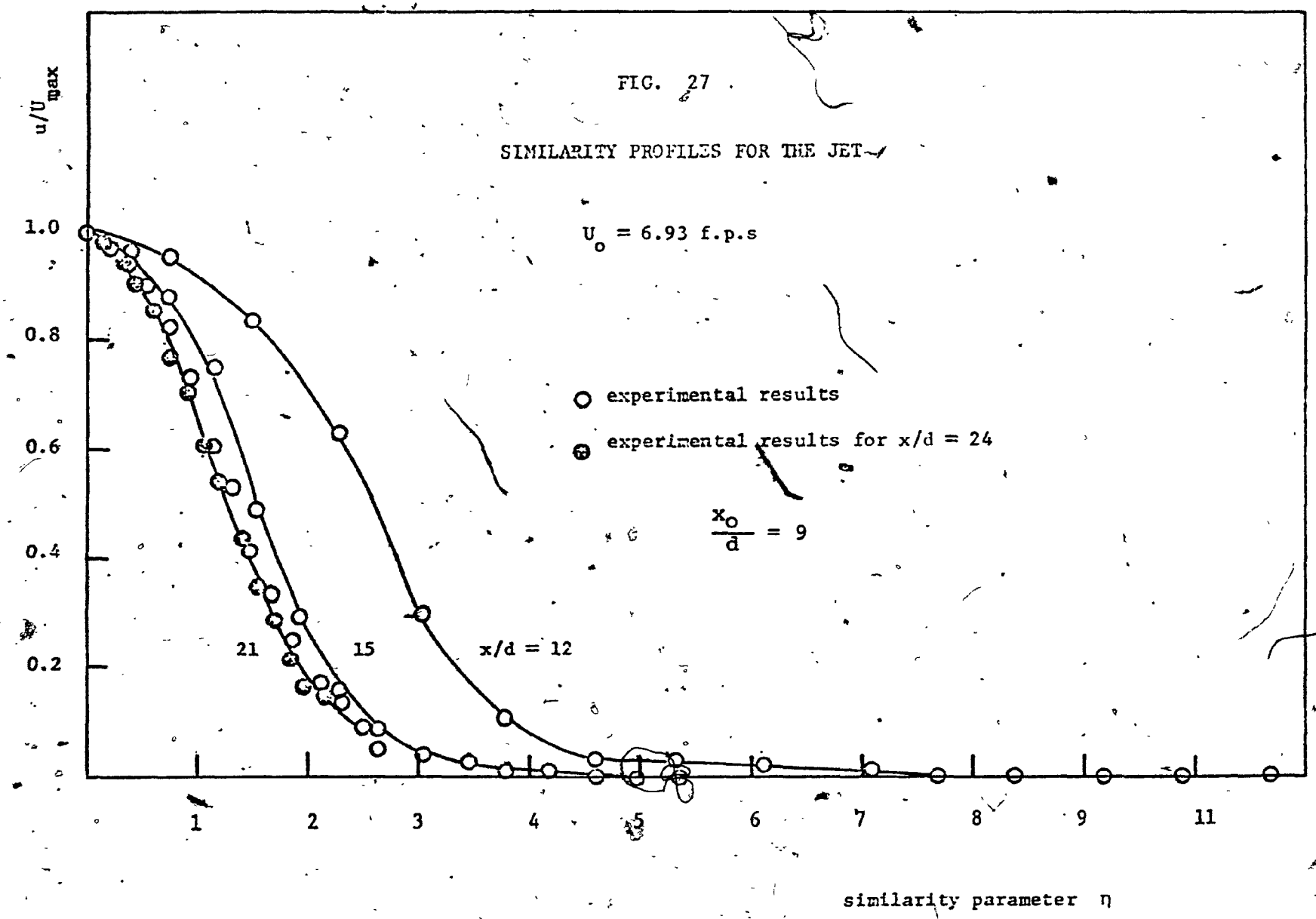

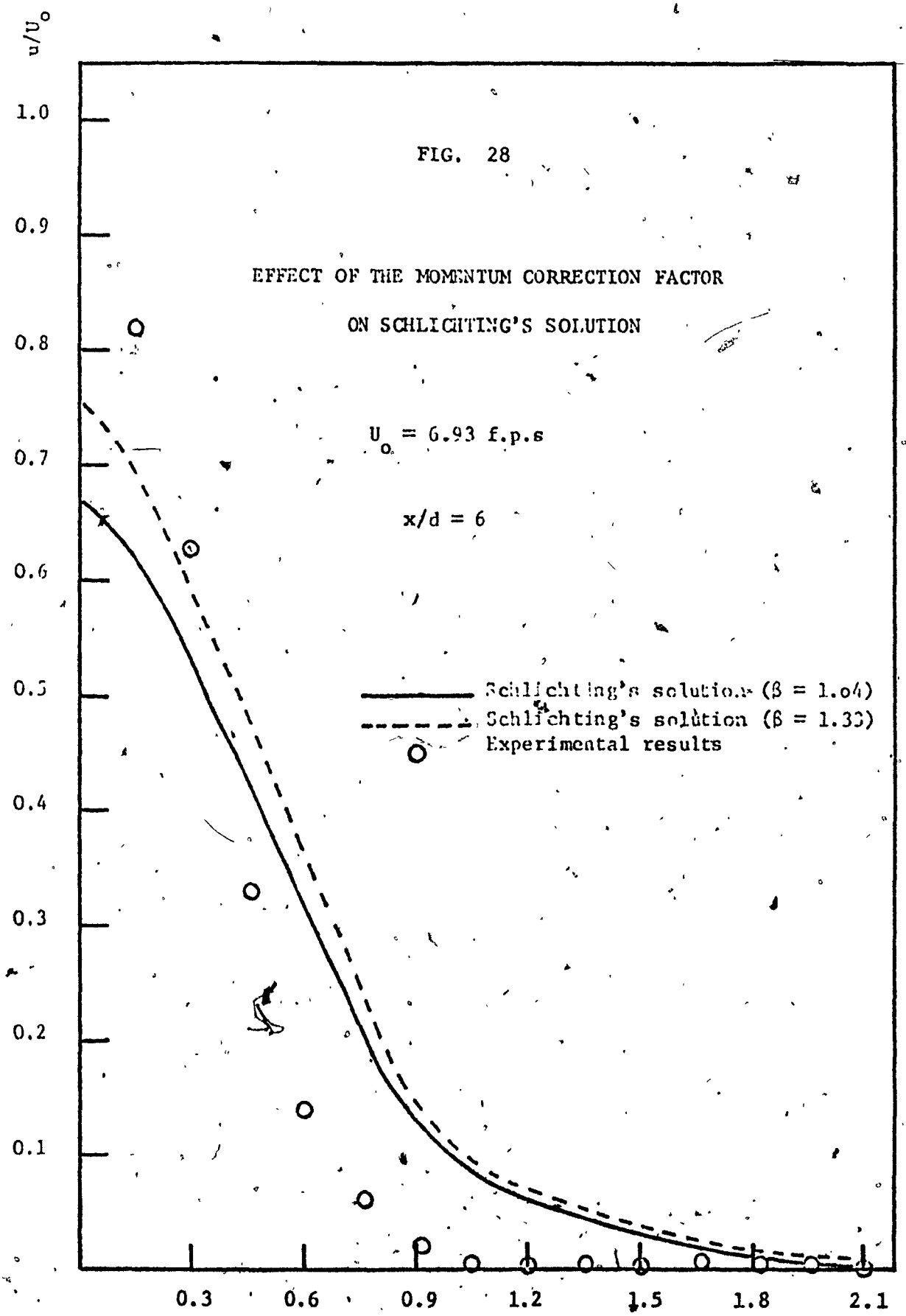

FIG. 28

EFFECT OF THE MOMENTUM CORRECTION FACTOR

ON SCHLICHTING'S SOLUTION

U_o = 6.93 f.p.s

x/d = 6

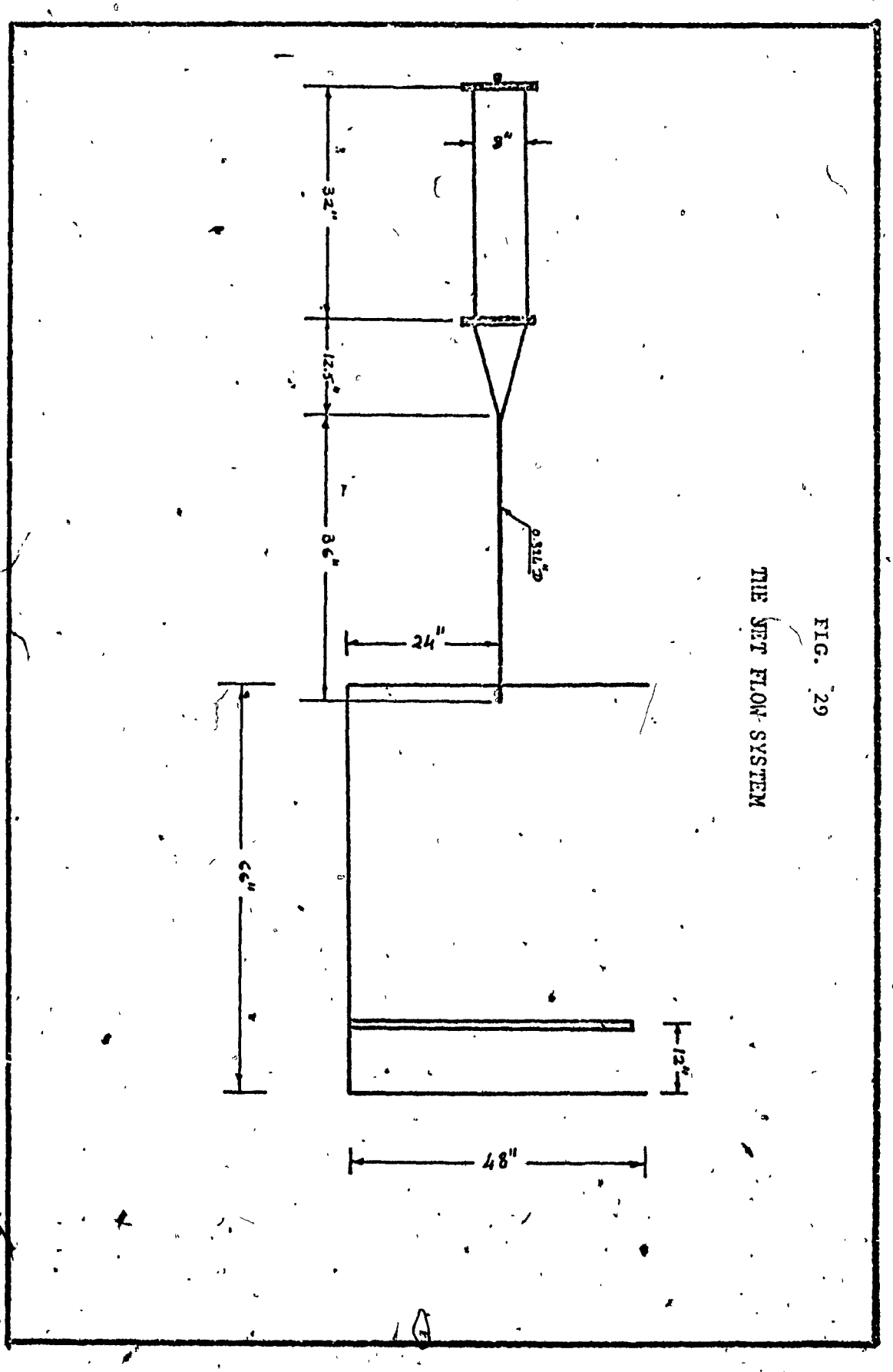

FIG. 29
THE JET FLOW SYSTEM

FIGURE 30

AXIS VELOCITY DECAY - LINEAR REGRESSION ANALYSIS

(EXPERIMENTAL RESULTS)

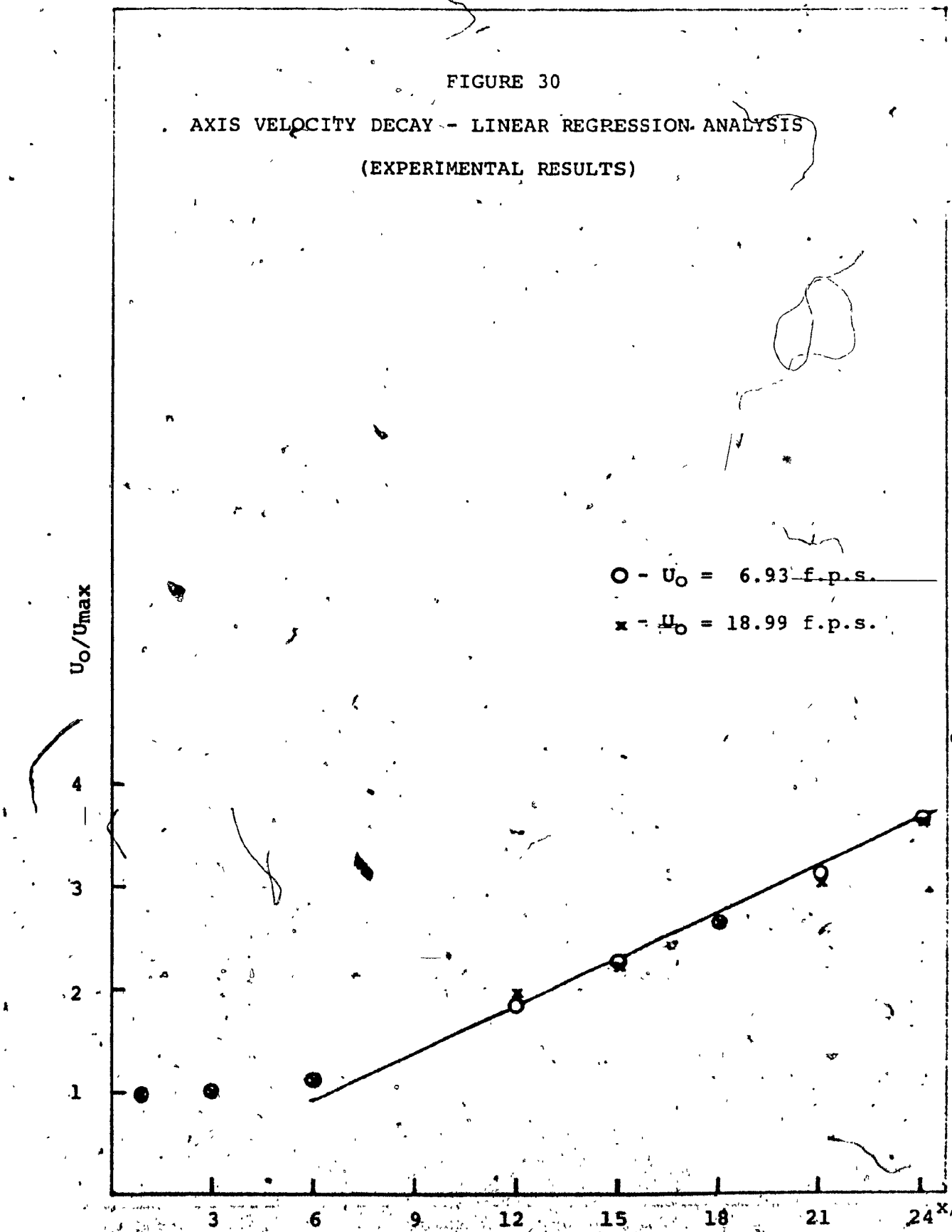

FIGURE 32

EXPERIMENTAL & THEORETICAL VELOCITY PROFILES

U_o = 6.93 f.p.s., Re = 1072

x/d = 1.57

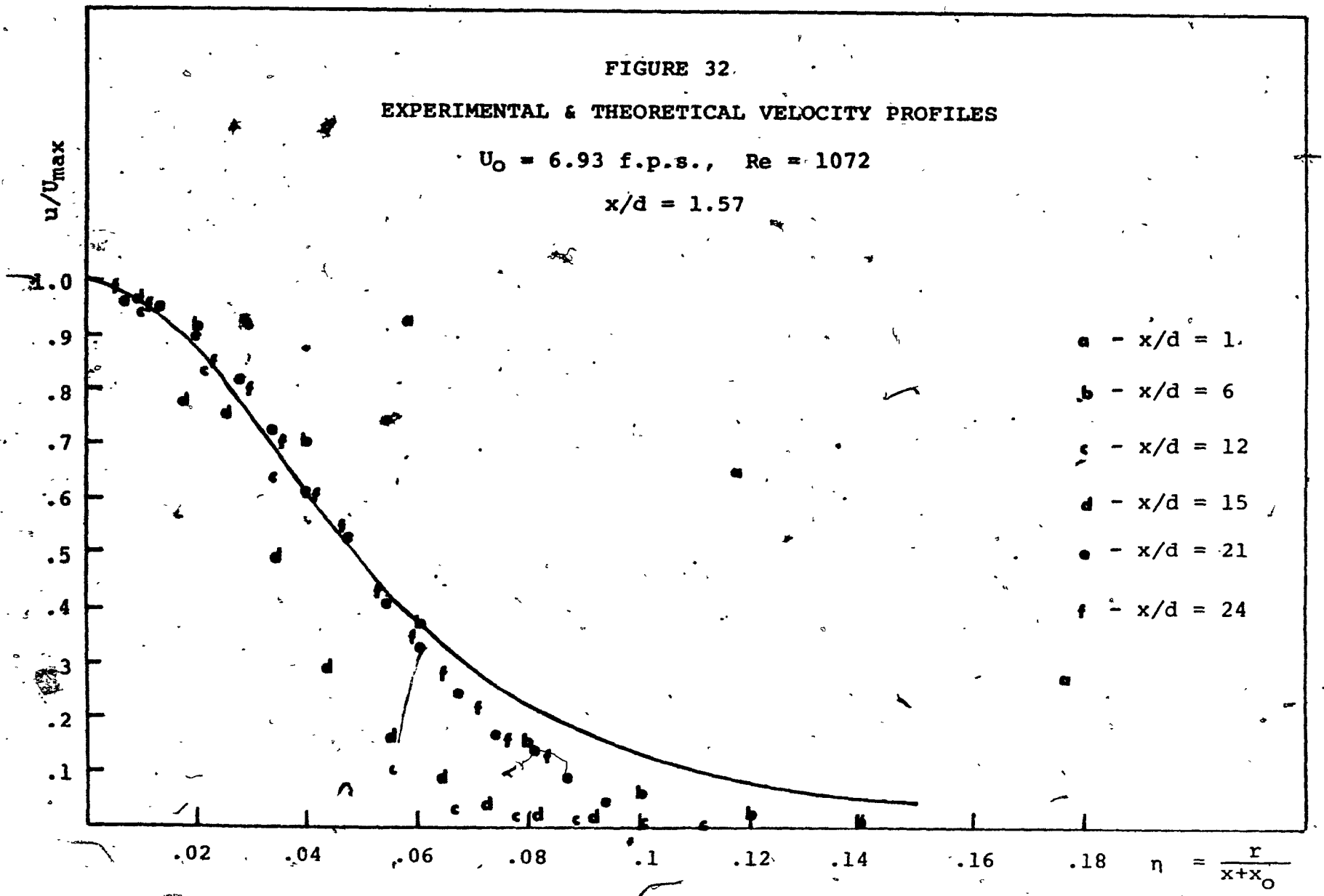

FIGURE 31

EXPERIMENTAL & THEORETICAL VELOCITY PROFILES

U_o = 18.99 f.p.s., Re = 2937

x/d = 2.31